CORROSION SCIENCE AND TECHNOLOGY, Vol.24, No.6(2025), pp.411~433 pISSN 1598-6462 / eISSN 2288-6524
[Research Paper] DOI: https://doi.org/10.14773/cst.2025.24.6.411

Eco-Friendly Corrosion Inhibition of Mild Steel in 1 M HCl Using *Trametes versicolor* (Turkey Tail Mushroom) Extracts: Experimental and Theoretical Insights

Qëndrim Ramshaj[1], Adelina Halili[2], Veprim Thaçi[3], Jeton Halili[3], Valbonë Mehmeti[4], Behar Baxhaku[5], Makfire Sadiku[3], Ilir Mazreku[1], Arianit Reka[6], and Avni Berisha[3,†]

[1]*Department of Biology, Faculty of Natural and Mathematics Science, University of Prishtina, 10000 Prishtina, Kosovo*
[2]*Kosovo Forensic Agency, 1000, Pristina, Kosovo*
[3]*Department of Chemistry, Faculty of Natural and Mathematics Science, University of Prishtina, 10000 Prishtina, Kosovo*
[4]*Faculty of Agriculture and Veterinary, University of Prishtina, Prishtina, 10000, Kosovo*
[5]*Department of Mathematics, Faculty of Natural and Mathematics Science, University of Prishtina, 10000 Prishtina, Kosovo*
[6]*Faculty of Natural Sciences and Mathematics, University of Tetova, Tetovo 1200, North Macedonia*
(Received April 22, 2025; Revised June 20, 2025; Accepted June 23, 2025)

In pursuit of greener corrosion control, this study evaluates Trametes versicolor (Turkey Tail Mushroom) extract as a corrosion inhibitor for mild steel in 1 M HCl. Using experimental and theoretical approaches, the extract achieved up to 92.1% inhibition efficiency at 800 mg/L, though efficiency declined with higher temperatures, suggesting predominantly physical adsorption with possible chemisorption. GC-MS/MS and FTIR analyses revealed various bioactive compounds—mainly flavonoids and polyphenols—containing functional groups like hydroxyl, carbonyl, and amine that promote protective film formation on the metal surface. UV-Vis spectroscopy confirmed iron-inhibitor complex formation, indicating chemical interactions at the interface. To support these results, DFT, MD, and MC simulations provided molecular-level insights into adsorption behavior, highlighting myricetin and rutin as key compounds with strong binding affinities and favorable electronic properties. A QSAR model with 22 molecular descriptors was developed to predict adsorption energies, identifying frontier orbital energies and surface area as major factors influencing inhibitor performance. These findings demonstrate the potential of T. versicolor extract as an eco-friendly corrosion inhibitor and offer valuable molecular insights for designing bio-based corrosion control strategies.

Keywords: *Trametes versicolor, Corrosion inhibition, Phytochemicals, Molecular dynamics simulations, Sustainable inhibitors*

1. Introduction

Iron and its alloys are widely utilized across various industries due to their strength, durability, and versatility [1-4]. However, when exposed to aggressive environments, they are highly susceptible to corrosion, which compromises structural integrity and functionality. One of the most effective strategies for mitigating corrosion is the use of inhibitors, which slow down the corrosion process and significantly reduce the degradation rate [5-9]. Traditionally, inorganic compounds such as phosphates, chromates, silicates, borates, tungstates, molybdates, and arsenates have been employed as corrosion inhibitors. These substances have also been incorporated into primers and protective coatings to enhance metal longevity [10,11]. However, their toxicity poses severe environmental and health risks, leading to growing concerns and regulatory restrictions on their use. In response to these challenges, the advancement of green chemistry has driven the search for environmentally friendly, non-toxic corrosion inhibitors. Natural compounds derived from plant and microbial sources have gained significant attention as sustainable alternatives for steel protection in acidic environments. The effectiveness of these bio-based inhibitors is attributed to their strong adsorption capabilities, facilitated by active molecular components such as

[†]Corresponding author: avni.berisha@uni-pr.edu

tannins, alkaloids, amino acids, and other organic compounds containing heteroatoms like sulfur (S), nitrogen (N), and oxygen (O) [12-15]. These functional groups act as reactive centers, enabling adsorption onto the metal surface and forming a protective film that acts as a barrier against corrosive agents. The inhibition efficiency of these compounds depends on the mechanical stability, structural integrity, and chemical properties of the adsorption layers formed under specific environmental conditions. With the increasing emphasis on sustainable industrial practices, research into bio-based inhibitors continues to expand, offering promising solutions for corrosion control while minimizing environmental impact.

Although numerous studies have explored various synthetic chemical inhibitors—including imidothiazoles [16], epoxy resins and monomers [7,17-20], Schiff bases [21], pharmaceutical compounds [22], nanomaterials [9-11], smart coatings [23] and a wide range of plant extracts [3,24-27] - research on mushroom-derived extracts as corrosion inhibitors for metals and alloys remains relatively limited. Despite their potential as eco-friendly and sustainable alternatives, the use of fungal extracts in corrosion protection has not been extensively investigated, leaving a gap in the exploration of bio-based inhibitors with unique biochemical properties and adsorption mechanisms. Suarez-Hernandez *et al.* [28], investigated the corrosion inhibition potential of *Ganoderma lucidum* (Reishi Mushroom) extract for carbon steel in 0.5 M H_2SO_4. Through weight loss measurements, they reported an inhibition efficiency of 92%, stressing the extract's strong protective capabilities. Ivušić [29] explored the corrosion inhibition potential of various fungal extracts derived from species such as *Lactarius volemus*, *Rozites caperata*, and *Boletus pinophilus* for carbon steel in a 0.5% NaCl solution. The study provided evidence of the effectiveness of these natural extracts in mitigating corrosion, further supporting the viability of fungi-derived bio-inhibitors as sustainable alternatives for protecting metals in chloride-rich environments. In an intriguing study, Pereira Monteiro *et al.* [30] utilized fungal biomass derived from cocoa bean shells (FBCS), produced through solid-state fermentation (SSF) with Penicillium roqueforti, as a natural corrosion inhibitor for carbon steel in a 0.5 M HCl solution. Their findings demonstrated a remarkable maximum inhibition efficiency of 93%, highlighting the potential of fungal-based biomass in corrosion protection of metals.

This study systematically explored the corrosion resistance of *Trametes versicolor* extract (TVE) on mild steel (MS) in a 1 M HCl environment using a combined experimental and theoretical approach. Gravimetric analysis was conducted to evaluate its inhibition efficiency, while computational methods - including density functional theory (DFT) calculations, molecular dynamics (MD) simulations, and Monte Carlo (MC) simulations - were employed to gain deeper insights into the inhibition mechanism. These theoretical investigations provided a detailed understanding of the molecular structures and adsorption behavior of key active compounds in the extract, correlating their chemical properties with the observed corrosion inhibition performance. The integration of experimental and computational techniques highlights the potential of this natural extract as a sustainable and effective corrosion inhibitor.

2. Methods

2.1 Mushroom collection and treatment

Samples of *Trametes versicolor* were collected in Gërmia Park, near Prishtina, from a *Fagus sylvatica* forest, specifically from fallen wood and branches. Prior to collection, specimens were photographed in situ and then carefully wrapped in aluminum foil. Collection was conducted with attention to maintaining the quality and purity of the samples. Only healthy fruiting bodies, free from visible contaminants, were selected. After collection, samples were gently cleaned to remove surface impurities such as dust and organic residues. The mushrooms were then dried under controlled conditions to preserve their bioactive compounds and prevent microbial growth. Once fully dried, the specimens were finely ground into a powder to facilitate the extraction process and subsequent experimental analyses.

2.2 Soxhlet Extraction Process

A 4 g sample of dried and finely pulverized *Trametes versicolor* mushroom was placed in a thimble and inserted into the Soxhlet extraction apparatus. Methanol was used as the extraction solvent, and the process was conducted

for 6 hours. Following extraction, the solvent volume was concentrated to 4 mL using a rotary evaporator and subsequently stored at -10 ºC. Prior to corrosion measurements and FTIR analysis, the extract underwent further evaporation to remove any residual solvent.

2.3 GC-MS/MS characterization of *Trametes versicolor* extract

Samples were analyzed using a GC-MS/MS system operating under the Slow100.m method. Separation was achieved on an Agilent DB-1 capillary column (12 m × 200 µm × 0.33 µm). The oven was programmed from 50 ºC (0.25 min hold) to 220 ºC at 65 ºC/min, then to 290 ºC at 40 ºC/min (5.38 min hold). Total run time was 9.99 min with helium as the carrier gas at 0.8 mL/min (constant flow). Injection was performed in pulsed split mode (100:1) at 290 ºC using a 1 µL injection volume. The inlet pulse pressure was 25 psi for 0.5 min. The MS transfer line was set to 290 ºC. The collision cell used helium (1.25 mL/min) and nitrogen (1.5 mL/min) as quench and collision gases, respectively.

2.4 FTIR measurements

The solid residues obtained from mushroom extracts after solvent evaporation were analyzed using FTIR spectroscopy. A Shimazdu instrument was employed to record spectra in the 4500–400 cm^{-1} range, using KBr pellets. These measurements were performed with a resolution of 2 cm^{-1}, and each spectrum was acquired over 500 scans to ensure high spectral accuracy.

2.5 Gravimetric tests

The mass loss measurement method offers a straightforward and cost-effective approach to evaluating corrosion inhibition, requiring minimal equipment [31-33]. This technique involves determining the change in mass of a surface sample after a 6-hour immersion in a corrosive solution, both in the presence and absence of the plant extract inhibitor, at a controlled temperature of 298 K. The metal surface is meticulously prepared before testing by sequential polishing with fine-grit sandpaper (ranging from 1200 to 100 grit) to eliminate surface imperfections and etching marks. Prior to immersion, the sample is thoroughly rinsed with distilled water and dried using a nitrogen stream to ensure consistency. The corrosion rate (C_R) and inhibition efficiency (μ_w) are then calculated using the following equations:

$$C_R = \frac{m_i - m_f}{A \times T} \quad (1)$$

$$\mu_W[\%] = \frac{C_R^0 - C_R^{0i}}{C_R^0} \times 100 \quad (2)$$

All gravimetric measurements were performed in triplicate to ensure experimental reproducibility. The reported values represent the mean of three independent trials, with variations between replicates not exceeding 2-3%. The standard deviation of mass loss measurements remained below 0.01 g, and the corresponding relative standard deviations (RSDs) were consistently under 3.5%, confirming the high precision and reliability of the experimental data.

2.6 Computational studies (DFT, MC and MD)

To optimize the molecular structures, the DMol^3 module within the Biovia Materials Studio (MatS) suite was employed, utilizing Density Functional Theory (DFT) calculations at the M06-L/DND level, incorporating the COSMO solvation model for solvent inclusion [34-36]. To investigate the adsorption behavior and interaction mechanisms between the inhibitor molecules and the mild steel (MS) surface, Monte Carlo (MC) and Molecular Dynamics (MD) simulations were conducted. The molecular species under study - **Rutin, Tentoxin, Ergosterol, Myricetin** - were modeled in interaction with the MS surface [37-40]. MC and MD simulations are widely recognized for their ability to predict adsorption configurations and quantify the interaction energy between inhibitor molecules and metallic surfaces [32,41,42].The Forcite module in the MatS package was employed to simulate the adsorption process of the inhibitors onto the Fe(110) surface, chosen due to its high stability among iron crystallographic planes. The system was constructed using a periodic simulation box with dimensions 24.8 Å × 24.8 Å × 8.2 Å, along with a 45 Å vacuum layer to prevent boundary effects. The Fe(110) surface was modeled as a multi-layered atomic slab to closely represent real-world metal interfaces [31,32,37,38]. In the computational system, a single inhibitor molecule

was introduced alongside 850 water molecules, 10 hydronium ions, and 10 chloride ions**,** effectively replicating the electrochemical environment. The NVT ensemble was applied in combination with the COMPASSIII force field [43-45], maintaining a temperature of 295 K**,** a time step of 1 fs**,** and a total simulation time of 800 picoseconds [20,46-51]. Due to the inherent challenges in directly characterizing the formation and density of thin inhibitor films at metal-corrodent interfaces, the MD method was utilized to approximate inhibitor film density over simulation steps [52,53]. Conventional experimental techniques have historically struggled to provide accurate density measurements for these protective films, reinforcing the necessity of computational methodologies in elucidating inhibitor behavior at the molecular level.

2.7 Multiple Regression Analysis – QSAR

Multiple regression analysis [54,55] was employed in this study to predict Monte Carlo adsorption energies based on structural features of the inhibitors, thereby constructing a robust QSAR [56] predictive model. Multiple linear regression extends simple linear regression to include more than one explanatory variable. The linear multiple regression equation is expressed as:

$$Y = A_0 + \sum_{s=1}^{n} A_s W_s \tag{3}$$

where

- Y – the dependent variable;
- $W_1, W_2, \ldots, W_n$ – the independent variables;
- n – the number of independent variables;
- $A_1, A_2, \ldots, A_n$ – the unknown **regression coefficients**.

The unknown coefficients are estimated based on n observation for the dependent variable Y, and for each of the independent variables W_i's where $i = 1, 2, \ldots, T$.

Let us first write the sample regression function as follows:

$$Y_P = A_0 = \sum_{s=1}^{n} A_s W_{sp} + \varepsilon_p; \; p = 1, 2, \ldots, T \tag{4}$$

where ε_p is the residual term, Y_p - the pth observation of the dependent variable $W_{11}, \ldots, W_{np}$ – the p-thobservation of the $W_1, W_2, \ldots, W_p$.

In our case:

W_1: Connolly surface area (Atom Volumes and Surfaces); W_2 : Connolly surface occupied volume (Atom Volumes and Surfaces); W_3: HOMO eigenvalue (VAMP Electrostatics); W_4: LUMO eigenvalue (VAMP Electrostatics); W_5: Total dipole (VAMP Electrostatics); W_6: Dipole x (VAMP Electrostatics); W_7: Dipole y (VAMP Electrostatics); W_8: Dipole z (VAMP Electrostatics); W_9: Mean polarizability (VAMP Electrostatics); W_{10}: Hydrogen bond donor (Fast Descriptors); W_{11}: Hydrogen bond acceptor (Fast Descriptors); W_{12}: AlogP (Fast Descriptors); W_{13}: Balaban index JX (Fast Descriptors); W_{14} : Balaban index JY (Fast Descriptors); W_{15}: Wiener index (Fast Descriptors); W_{16}: Zagreb index (Fast Descriptors); W_{17}: Molecular area (vdW area) (Spatial Descriptors); W_{18}: Molecular volume (vdW volume) (Spatial Descriptors); W_{19}: Ellipsoidal volume (Spatial Descriptors); W_{20}: Dipole moment (magnitude) (Spatial Descriptors); W_{21}: Dipole moment X (Spatial Descriptors); W_{22}: Dipole moment Y (Spatial Descriptors); Y: Eads.

We can use a least squares technique to calculate estimates of $\hat{A}_0, \hat{A}_1, \ldots, \hat{A}_n$ of the coefficients $A_1, A_2, \ldots, A_n$. This amounts to minimizing the expression:

$$E = \sum_{p=1}^{T} [Y - (\hat{A}_0 + \hat{A}_1 W_{1p} + \ldots + \hat{A}_n W_{np})]^2 = \sum_{p=1}^{T} \varepsilon_p$$

Taking the partial derivatives of E with respect to $\hat{A}_0$, $\hat{A}_1$, …, $\hat{A}_n$, that is $\frac{\partial E}{\partial \hat{A}_0}, \frac{\partial E}{\partial \hat{A}_1}, \ldots, \frac{\partial E}{\partial \hat{A}_n}$ and setting them equal to zero, gives the following set of equations(called the normal equations):

$$T\hat{A}_0 + \left(\sum_{p=1}^{T} W_{1p}\right)\hat{A}_1 + \ldots + \left(\sum_{p=1}^{T} W_{1p}\right)\hat{A}_p = \sum_{p=1}^{T} Y_p \tag{5}$$

$$\left(\sum_{p=1}^{T} W_{1p}\right)\hat{A}_0 + \left(\sum_{p=1}^{T} W_{1p}^2\right)\hat{A}_1 + \ldots + \left(\sum_{p=1}^{T} W_{1p} W_{np}\right)\hat{A}_p = \sum_{p=1}^{T} Y_p W_p \tag{6}$$

$$\left(\sum_{p=1}^{T} X_{2p}\right)\hat{A}_0 + \left(\sum_{p=1}^{T} W_{1p} W_{2p}\right)\hat{A}_1 + \ldots + \left(\sum_{p=1}^{T} W_{2p} W_{np}\right)\hat{A}_p = \sum_{p=1}^{T} W_{2p} Y_p \tag{7}$$

⋮ ⋮ ⋮

$$\left(\sum_{p=1}^{T} W_{np}\right)\hat{A}_0+\left(\sum_{p=1}^{T} W_{1p}W_{np}\right)\hat{A}_1+\ldots+\left(\sum_{p=1}^{T} W_{np}^2\right)\hat{A}_p=\sum_{p=1}^{T} W_{np}Y_p \quad (8)$$

The above system of equations can be written in matrix form:

$$M\hat{A} = N \text{ Equation} \quad (8)$$

where

$$M=\begin{bmatrix} T & \sum_{p=1}^{T}W_{1p} & \ldots & \sum_{p=1}^{T}W_{1p} \\ \sum_{p=1}^{T}W_{1p} & \sum_{p=1}^{T}W_{1p}^2 & \ldots & \sum_{p=1}^{T}W_{1p}W_{np} \\ \vdots & \vdots & \vdots & \vdots \\ \sum_{p=1}^{T}W_{np} & \sum_{p=1}^{T}W_{1p}W_{np} & \ldots & \sum_{p=1}^{T}W_{np}^2 \end{bmatrix},\ A=\begin{bmatrix} A_0 \\ A_1 \\ \vdots \\ A_n \end{bmatrix} \text{ and } N=\begin{bmatrix} \sum_{p=1}^{T}Y_p \\ \sum_{p=1}^{T}W_{1p}W_p \\ \vdots \\ \sum_{p=1}^{T}W_{np}Y_p \end{bmatrix}$$

Retention time [min]	Relative Concentration [%]	Compound name
2.960	**17.860**	**Rutin**
1.866	**12.690**	**Tentoxin**
5.880	**10.860**	**Ergosterol**
2.652	**8.310**	**Myricetin**
4.061	5.440	D-Glucosyl-ß-1,1'-N-palmitoyl-D-erythro-sphingosine
5.695	4.380	Meleagrin
1.257	2.970	Dulcitol
1.667	2.300	Stachydrine
2.050	1.810	Kojic Acid
1.531	1.420	2-azainosine
2.597	0.910	Ergocorninine
2.502	0.640	Elaidic Acid
1.838	0.480	2,4-Di-tert-butylphenol

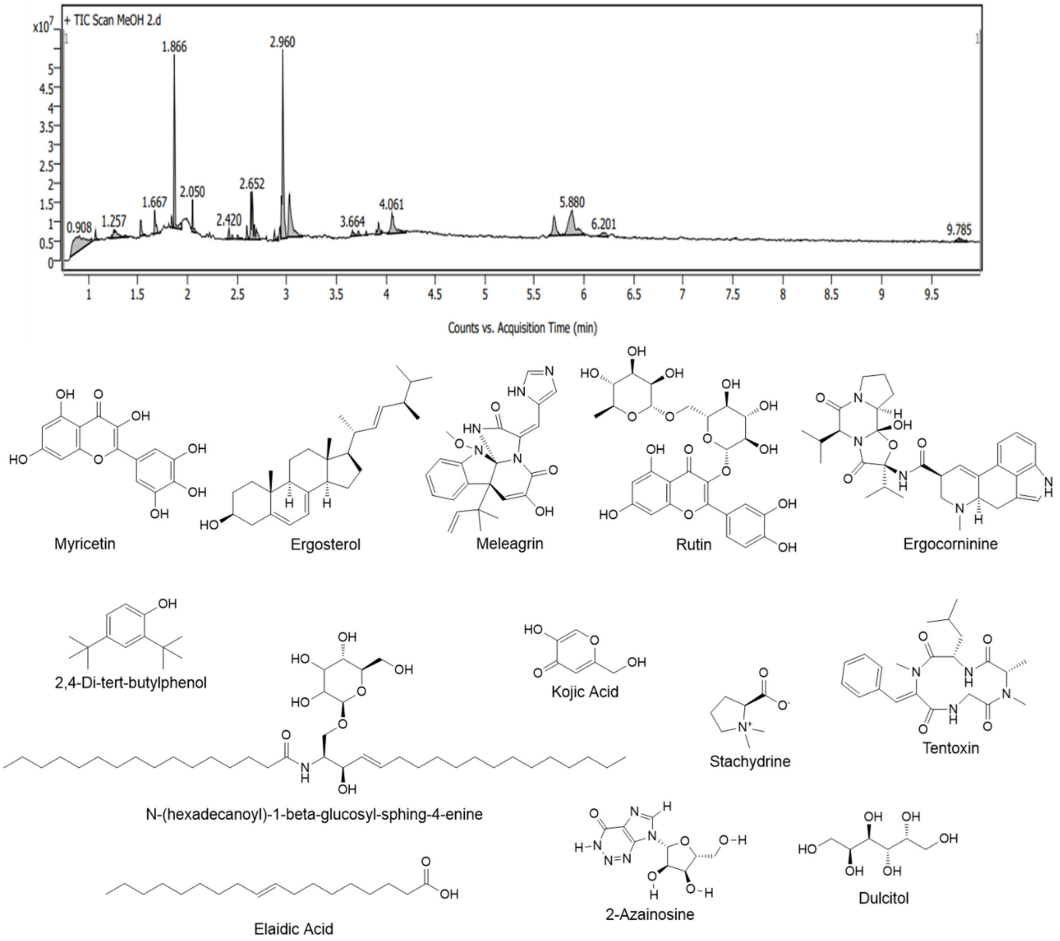

Fig. 1. Chromatogram of the *Trametes versicolor* extract (TVE) obtained through gas chromatography-tandem mass spectrometry (GC-MS/MS); The figure highlights the most representative bioactive compounds detected, along with their chemical structures and relative concentrations

N is a symmetric matrix.

We can obtain estimates for the coefficients $\hat{A}_0, \hat{A}_1, \ldots, \hat{A}_n$ by successive elimination or by solving for the inverse of N. That is

$$A = M^{-1}N \tag{10}$$

where M^{-1} – is the inverse matrix of the matrix M.

After solving for $\hat{A}_0, \hat{A}_1, \ldots, \hat{A}_n$, the estimates of the dependent variable observations $\hat{Y}_p$ can be obtained as follows:

$$\hat{Y}_p = \hat{A}_0 = \sum_{s=1}^{n} \hat{A}_s W_{sp}; \; p = 1, 2, \ldots, T \tag{11}$$

3. Results and Discussion

3.1 Chemical constituents in TVE

The analysis of the *Trametes versicolor* extract (TVE) was carried out using gas chromatography-tandem mass spectrometry (GC-MS/MS) to identify and quantify the bioactive compounds present. The resulting chromatogram, highlighting the most representative compounds, along with their chemical structures and relative concentrations, is presented in Fig. 1.

The TVE contains a diverse range of bioactive compounds, including: Rutin, Tentoxin, Ergosterol, Myricetin, D-Glucosyl-β-1,1'-N-palmitoyl-D-erythro-sphingosine, Meleagrin, Dulcitol, Stachydrine, and Kojic Acid, among others. These compounds exhibit structural features such as conjugated double bonds, polar functional groups (hydroxyl, carbonyl, and amine groups), and heteroatoms (oxygen, nitrogen, and sulfur). Due to their molecular architecture, these constituents may interact with metallic surfaces, potentially forming a protective layer that hinders oxidation and metal dissolution, thereby acting as corrosion inhibitors. Their inhibition efficiency potential could be attributed to adsorption on metal surfaces.

3.2 FTIR characterization

To identify the chemical constituents, present in the TVE, Fourier Transform Infrared (FTIR) spectroscopy was conducted at 25 ºC, with the corresponding spectrum illustrated in Fig. 2.

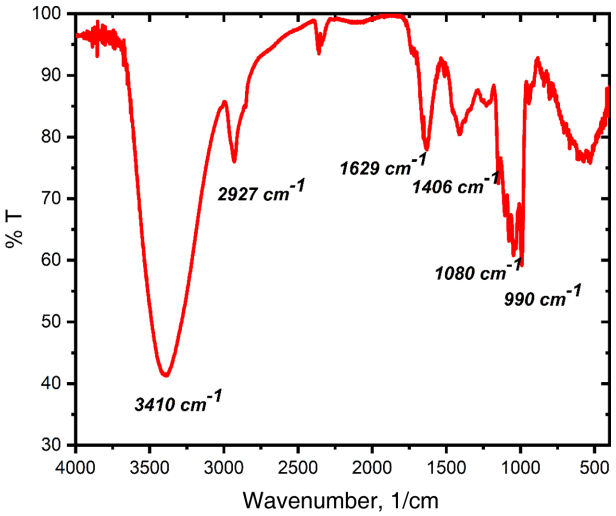

Fig. 2. FTIR spectra of the *Trametes versicolor* extract (TVE)

The spectrum obtained at 25 ºC reveals a distinct absorption peak at 3410 cm^{-1}, characteristic of O-H functional groups, which are known to play a role in metal passivation. Furthermore, a prominent signal appears at 2927 cm^{-1}, indicative of N-H bonds, most likely associated with amine groups (in molecules like: meleagrin, ergocornine). Such compounds are widely recognized for their effectiveness as corrosion inhibitors, particularly for iron and steel in acidic environments. A pronounced signal at 1629 cm^{-1} corresponds to the C=O bond, serving as strong evidence for the resence of carboxylic acid moieties in the extract. Additionally, a distinct absorption band at 1395 m^{-1} is associated with C-C vibrations, a characteristic feature of aromatic ring structures. The signal detected at 1046 cm^{-1} is assigned to C-N stretching, indicative of amine or amide functional groups, while the absorption peak near 990 cm^{-1} corresponds to the vibrational modes of C-H bonds.

3.3 UV-VIS

Fig. 3 illustrates the UV-Vis spectra of TVE before and after immersing mild steel samples. According to previous studies, any shift in the position or intensity of the maximum absorbance peak in a UV-Vis spectrum suggests the formation of a complex between the interacting substances in the solution. In the spectrum, two key absorption bands are observed.

The first, appearing in the 200-215 nm range,

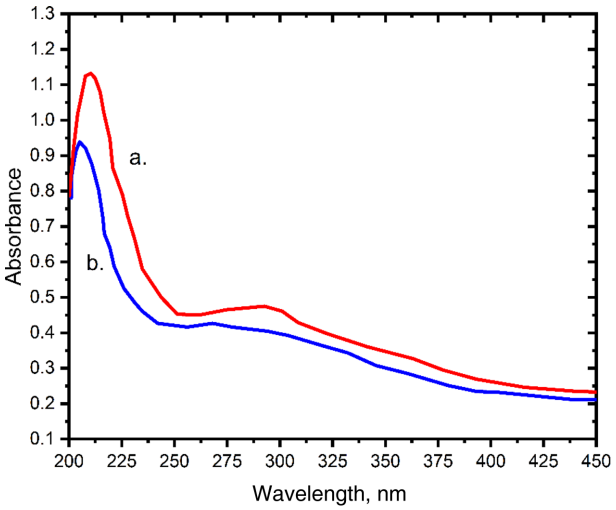

Fig. 3. UV-vis spectra of TVE before (a) and after immersion (b) of mild steel

corresponds to n–σ* and π–π* electronic transitions, which are characteristic of functional groups such as carboxyl, ester, carbonyl, and amines [57]. The second absorption band, located around 260-280 nm, is attributed to π–π* transitions commonly found in aromatic and polyaromatic compounds within conjugated molecular structures. After immersion of the mild steel, both absorption peaks exhibited a blue shift (a shift to lower wavelengths) compared to the original TVE spectrum. This shift indicates the formation of a complex between the extract's active molecules and Fe^{2+} ions, further supporting the extract's role in corrosion inhibition.

3.4 Gravimetric test

3.4.1 Effect of TVE extract concentration

Fig. 4 presents the results of the gravimetric analysis, illustrating how different concentrations of TVE extract influence key parameters such as corrosion rate (C_R) and inhibition efficiency at 298 K. As shown in Fig. 2, *TVE* demonstrates remarkable effectiveness in inhibiting mild steel (MS) corrosion in a 1 M HCl solution, achieving a maximum inhibition efficiency of 92.1% at a concentration of 800 mg/L. This high level of protection is attributed to the adsorption of the extract's components, which facilitate the formation of a robust organic layer on the metal surface. This protective barrier significantly reduces the impact of aggressive ions, thereby minimizing corrosion in the acidic environment [58-60].

The gravimetric analysis indicates that the inhibitor

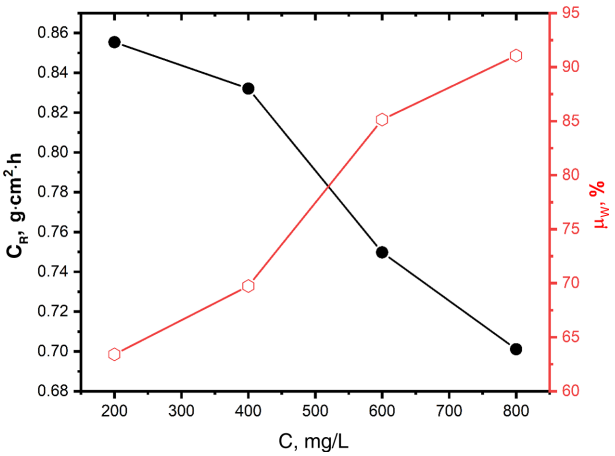

Fig. 4. The development of inhibiting efficiency and C_R in 1 M HCl without and with TVE in the c= [200-800 mg/L]

molecules in the extract readily adsorb onto the metal surface, primarily due to the presence of multiple active sites. These include oxygen atoms (O) and π-bonds, which facilitate strong interactions with the metal, enhancing the formation of a protective barrier that mitigates corrosion [60].

3.4.2 Effect of immersion time

As shown in Fig. 5, the presence of the extract in the 1 M HCl solution significantly reduces the corrosion rate (C_R) over an extended immersion period. Notably, after 24 hours, the CR stabilizes while maintaining a relatively high inhibition efficiency. This behavior can be attributed to the displacement of water molecules at the metal-electrolyte interface by the organic molecules in the

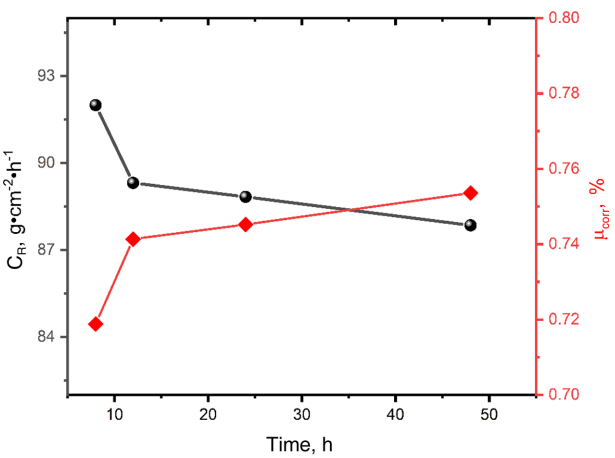

Fig. 5. The development of inhibiting efficiency and C_R in 1 M HCl without and with TVE at different immersion times [c=800 mg/L]

extract, which adsorb onto the surface. Consequently, the formation of a stable and durable protective coating effectively minimizes corrosion, ensuring sustained inhibition over time [61-63].

3.4.3. Effect of temperature and different values of the thermodynamic parameters

To understand the thermodynamic reactivity of the TVE extract on the catalytic sites of steel when changing the temperature parameter, we performed mass loss studies of MS in 1M HCl acid without and with inhibitor, at a temperature from 308 to 328 K for immersion time of 8 h and at a concentration of 800 mg/L in which the inhibition efficiency reaches the maximum value at T = 35 ºC. The results of this study are presented in Table 1.

To further elucidate the thermodynamic nature of the adsorption process, the standard free energy of adsorption ($\Delta G^{o}_{ads.}$) was calculated using the Langmuir adsorption model based on inhibition efficiencies at a fixed inhibitor concentration (800 mg/L) and varying temperatures. The surface coverage (θ) values were derived from the experimental inhibition efficiencies and used to estimate the adsorption equilibrium constant ($K_{ads.}$) at 308, 318, and 328 K. The resulting $\Delta G^{o}_{ads.}$ values were –31.87, –31.95, and –30.60 kJ/mol, respectively. These negative values confirm that the adsorption of *Trametes versicolor* extract components onto the mild steel surface is a spontaneous process. Furthermore, the magnitudes of $\Delta G^{o}_{ads.}$ fall within the typical range for physisorption (-20 to -40 kJ/mol), indicating that the adsorption is primarily governed by electrostatic interactions and hydrogen bonding, possibly supported by very weak chemisorptive contributions [12-15]. The slight decrease in $\Delta G^{o}_{ads.}$ at higher temperatures suggests a decline in adsorption strength, which is consistent with the observed reduction in inhibition efficiency due to desorption effects.

To have a clear concept on the evolution of electrochemical reactions involved during the process of inhibiting the corrosion of metals. The determination of thermodynamic quantities such as the enthalpy of adsorption ΔH^{o}_{ads}, the activation energy E^{0}_{act} and the entropy ΔS^{o}_{ads}, allow us to know the type and mechanism of adsorption.

The apparent E^{0}_{act} was determined from the slopes of ln (C_R) versus 1000/T shown in Fig. 6. The E^{0}_{act} are therefore determined by the following relationship:

$$\ln(C_R) = \ln(A) - \frac{E^{0}_{act}}{RT} \quad (12)$$

At the same time, the values of free enthalpy and the entropy of adsorption are thus determined by the following relation [64,65]:

$$\ln\left(\frac{C_R}{T}\right) = \ln\left(\frac{R}{Nh}\right) + \frac{\Delta S^{o}_{ads}}{R} - \frac{\Delta H^{o}_{ads}}{RT} \quad (13)$$

Fig. 3 gives the variation of $\ln\left(\frac{C_R}{T}\right)$ depending on the opposite of the absolute temperature in the form of straight lines with temperature slope $-\frac{\Delta H^{o}_{ads}}{RT}$ and extrapolation of these lines gives the values of $\ln\left(\frac{R}{Nh}\right) + \frac{\Delta S^{o}_{ads}}{R}$ from which the values of ΔH^{o}_{ads} are calculated.

Table 1 indicates that as the temperature increases, the inhibition efficiency of the TVE extract decreases, while the corrosion rate (C_R) rises. This trend suggests that the inhibitor gradually desorbs from the MS surface at higher temperatures. Additionally, the activation energy in the presence of the inhibitor is higher than in its absence, implying that the adsorption mechanism is predominantly

Table 1. Different values of the thermodynamic adsorption parameters of the system in the presence and absence of the TVE extract

Inhibitor	308K		318K		328K		E^{0}_{act} [kJ/mol]	ΔH^{0}_{act} [kJ/mol]
	C_R [g/cm^2·h]	μ_W [%]	C_R [g/cm^2·h]	μ_W [%]	C_R [g/cm^2·h]	μ_W [%]		
1M HCl	1.2901	-	1.997	-	3.812	-	45.39	42.75
800 mg/L of TVE	0.1484	92.0154	0.2841	88.9208	0.8211	77.213	71.64	68.99

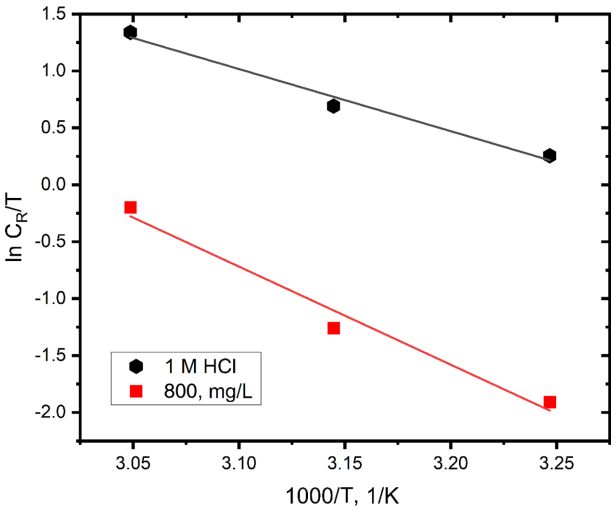

Fig. 6. Arrhenius transition curves for the C_R of MS coupons immersed in the 1M HCl acid solution without and with the TVE

physisorption. This means the inhibitor interacts with the metal surface through electrostatic forces rather than forming strong chemical bonds.

The positive sign of enthalpy ΔH^{o}_{ads}, as determined from Fig. 6, indicates that the corrosion process slows down significantly after the addition of the TVE extract. The higher enthalpy value in the presence of the inhibitor suggests that the adsorption of TVE onto the metal surface requires energy, making the dissolution process less favorable. This confirms that metal dissolution in this system is endothermic, meaning it absorbs heat to proceed.

3.6 DFT

To begin with, the process started by performing a conformer search using Random Sampling, generating a pool of 1000 possible structures [66]. This search was guided by the COMPASS III force field, which helped estimate the initial energies of the conformers. The primary goal at this stage was to identify the structure with the lowest possible energy—serving as an ideal starting point for the subsequent DFT calculations and helping streamline their computational cost. As illustrated in Fig. 7, the DFT workflow began by selecting the conformer with the minimum energy from the generated set.

To generate the sigma-profile charge density curve, the COSMO model employs partially charged atomic nuclei to represent the electrostatic potential across the molecular surface [67].

When an inhibitor dissolves in water, it engages in hydrogen bonding - acting either as an H-bond donor or acceptor - with surrounding water molecules. This behavior plays a crucial role in determining the solubility of the inhibitor. As illustrated in Fig. 8, all inhibitors display peaks in their screening charge density profiles beyond +0.01 and below –0.01, indicating that they exhibit both H-bond donating and accepting capabilities.

Fig. 9 provides insight into the electronic behavior of the inhibitors. For the inhibitors, the highest occupied molecular orbital (HOMO) is localized on one side of the O-containing ring, while the lowest unoccupied molecular

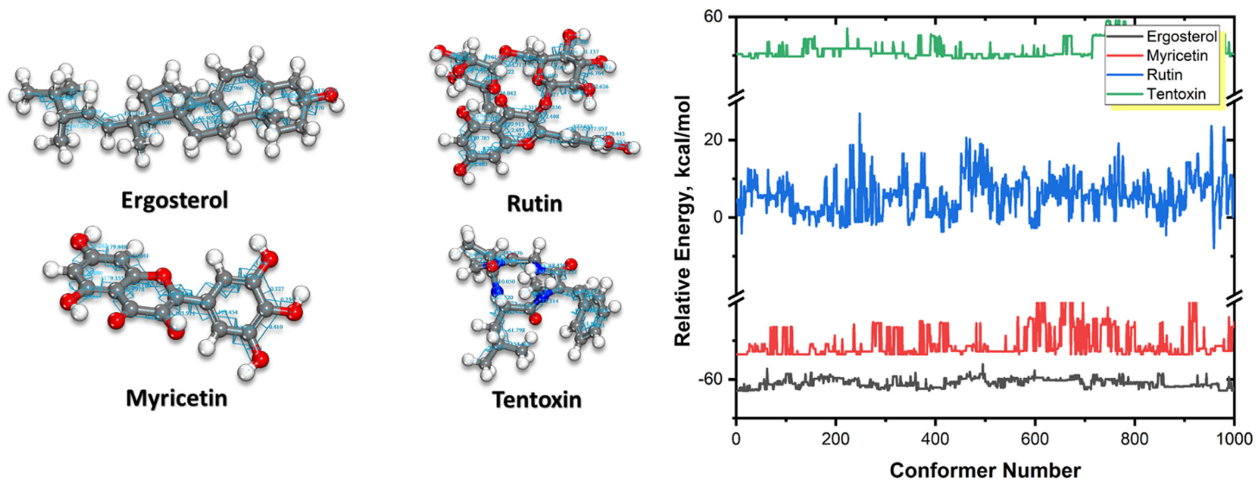

Fig. 7. The energy profile of the conformer search and the lowest energy structures of the inhibitors

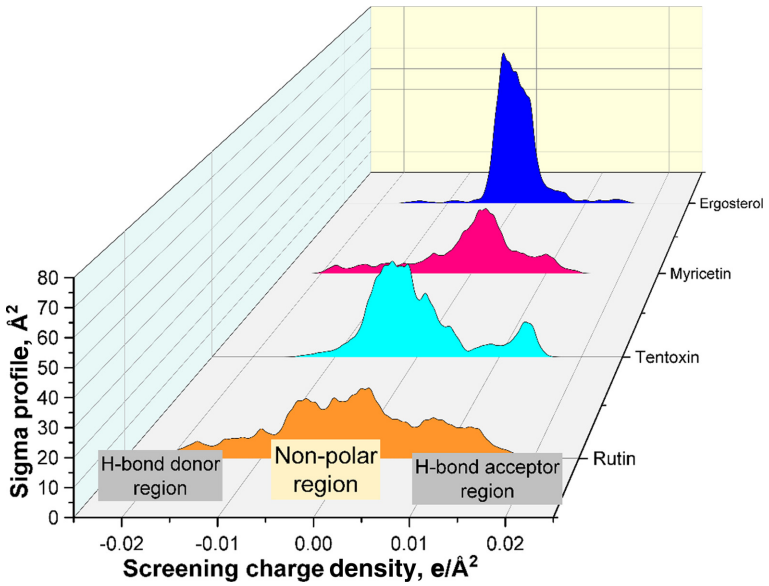

Fig. 8. COSMO profiles of the inhibitors

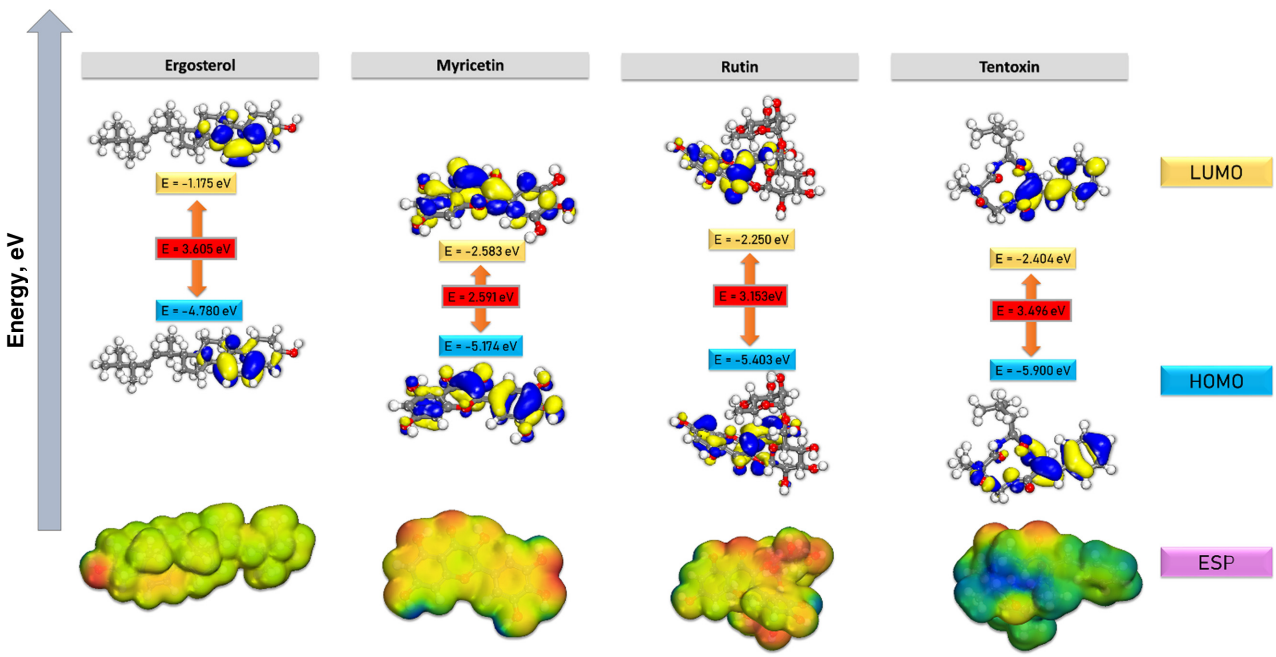

Fig. 9. HOMO, LUMO, and ESP of the inhibitors

orbital (LUMO) is positioned on the opposite side. This spatial separation suggests directional electron donation and acceptance, which is essential for their interaction with the metal surface [52,53]. The presence of heteroatoms like oxygen (O) and nitrogen (N) enhances this interaction, as their lone pair electrons can coordinate with the empty d-orbitals of iron. This lone pair exchange significantly boosts the molecule's adsorption strength on the metal surface, thereby enhancing its protective efficacy. The electrostatic potential (ESP) maps generated using DMol^3 reveal distinct differences in the charge distribution of the investigated molecules, providing valuable insights into their potential as corrosion inhibitors. Ergosterol exhibits a largely neutral surface with minimal red or blue regions, indicating low polarity and limited active sites for interaction with metal surfaces.

In contrast, myricetin and rutin display pronounced regions of negative and positive potential, particularly around hydroxyl and aromatic moieties, suggesting a strong capacity for electron donation and adsorption onto metal surfaces. Notably, rutin shows an extensive polar surface with highly localized charge densities, highlighting its superior potential as a corrosion inhibitor. Tentoxin, while demonstrating moderate ESP variation near its amide and carbonyl functionalities, presents fewer reactive zones compared to the flavonoids. Overall, the ESP analysis underscores the enhanced inhibition efficiency of rutin and myricetin due to their rich electron density distribution and polar functional groups, whereas ergosterol and tentoxin appear less favorable for strong surface interactions. The DFT-derived descriptors (Table 2) proved to be very important in elucidating the electronic and structural features of the molecules acting as corrosion inhibitors. The equations used for these calculations are provided elsewhere. The efficiency of a molecule as a corrosion inhibitor is closely related to its electronic properties, particularly its frontier molecular orbitals and global reactivity descriptors derived from density functional theory (DFT). Among the studied compounds - ergosterol, myricetin, rutin, and tentoxin - distinct variations in electronic behavior were observed, suggesting different mechanisms and degrees of interaction with metallic surfaces.

The energy of the highest occupied molecular orbital (HOMO) indicates the electron-donating capability of the molecule, with ergosterol exhibiting the highest HOMO value (-4.78 eV), implying a greater tendency to donate electrons to vacant d-orbitals of metal atoms and form coordinate bonds. However, its relatively large HOMO–LUMO gap (3.605 eV), high global hardness (1.80 eV), and low softness (0.55 eV) suggest limited reactivity, classifying ergosterol as a moderately effective inhibitor, primarily through donor-based interactions. In contrast, myricetin displayed the most favorable electronic characteristics for corrosion inhibition. It possessed the lowest HOMO–LUMO energy gap (2.591 eV), indicating higher molecular reactivity and readiness to interact with the metal surface. Furthermore, its high electronegativity (3.88 eV), low hardness (1.29 eV), and the highest global softness (0.77 eV) enhance its ability to participate in charge transfer processes. Myricetin also showed the highest global electrophilicity index (5.81 eV), electrodonating power (7.91 eV), and electroaccepting power (4.03 eV), all pointing toward its strong dual nature as both electron

Table 2. DFT-derived electronic descriptors of four selected TVE extracts, highlighting their potential as corrosion inhibitors

Parameter	Ergosterol	Myricetin	Rutin	Tentoxin
HOMO	-4.7800	-5.174	-5.403	-5.900
LUMO	-1.1750	-2.583	-2.25	-2.404
ΔE(HOMO-LUMO)	3.605	2.591	3.153	3.496
Ionization energy (I)	4.7800	5.174	5.403	5.900
Electron affinity A)	1.1750	2.583	2.25	2.404
Electronegativity (X)	2.9775	3.8785	3.8265	4.152
Global hardness (η)	1.8025	1.2955	1.5765	1.748
Chemical potential (π)	-2.9775	-3.8785	-3.8265	-4.152
Global softness (σ)	0.5548	0.771903	0.634317	0.572
Global electrophilicity (ω)	2.4592	5.805775	4.643864	4.931
Electrodonating (ω-) power	4.1733	7.906962	6.754176	7.226
Electroappcepting (ω+) power	1.1958	4.028462	2.927676	3.074
Net electrophilicity (Δω+-)	0.9562	3.901991	2.77962	2.935
Fraction of transferred electrons (ΔN)	0.0700	-0.25029	-0.18918	-0.264
Energy from Inhb to Metals (ΔN)	0.0088	0.081156	0.056424	0.122
ΔE back-donation	-0.4506	-0.32388	-0.39413	-0.437

donor and acceptor. This is further supported by its high net electrophilicity ($\Delta\omega^{+-} = 3.90$ eV) and favorable energy exchange with the metal surface ($\Delta N = 0.081$), making it the most promising candidate among the tested molecules. Rutin presented intermediate behavior with a HOMO–LUMO gap of 3.15 eV, global softness of 0.63 eV, and moderate electrophilicity (4.64 eV). While its capacity to donate and accept electrons was notable, its values were consistently lower than those of myricetin, implying a lesser, albeit still significant, inhibition performance.

Tentoxin, on the other hand, exhibited characteristics indicative of strong electron-accepting ability. It had a high electronegativity (4.15 eV), considerable electrophilicity (4.93 eV), and the most negative value for the fraction of transferred electrons ($\Delta N = -0.264$), suggesting that it can act as an electron sink during adsorption. Although it does not match myricetin in softness or reactivity, tentoxin's balanced donor-acceptor properties and favorable interaction energy with the metal support its potential as an effective corrosion inhibitor. The DFT descriptors suggest that all four compounds possess the necessary electronic features to function as corrosion inhibitors [68-70], with myricetin emerging as the most potent due to its high reactivity and balanced electronic characteristics. Tentoxin also demonstrates strong potential, particularly through its electron-accepting capability, followed by rutin and ergosterol, which exhibit moderate inhibition efficiency properties primarily via electron donation.

3.7 MC and MD

To gain deeper insights into material corrosion, researchers frequently employ Monte Carlo (MC) simulations using the Forcite module within the BIOVIA software suite. This method enables atomistic modeling of how ions and molecules interact with metal surfaces under corrosive conditions. Leveraging quantum mechanical (QM) calculations, Forcite accurately describes the electronic structure and adsorption behavior of both corrosive species and inhibitor molecules, offering a detailed view of the processes that govern corrosion at the atomic scale [21,39,71,72]. The simulations generate extensive data on interaction energies and molecular geometries, which can be statistically analyzed to evaluate the material's response to environmental factors, such as the presence of aggressive media [20,46,73,74]. This approach provides a powerful framework for understanding corrosion mechanisms and assessing the effectiveness of potential inhibitors.

The simulation begins with the setup of the simulated medium and its surrounding environment, followed by the random selection of ions or molecules to participate in surface adsorption events, based on the local probability

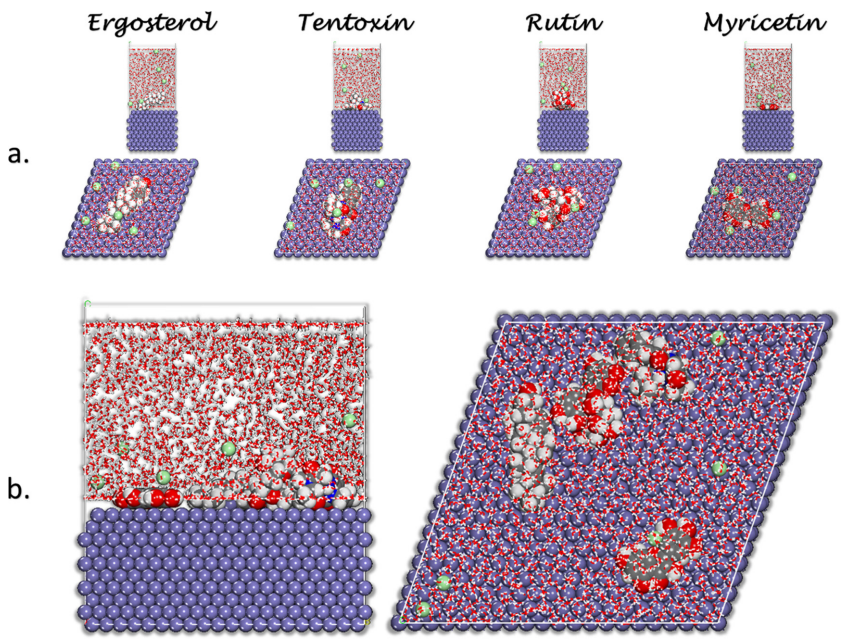

Fig. 10. MD poses for: a. single inhibitors and b. all four inhibitors interacting with mild steel surface

of corrosion. As shown in Fig. 10, the inhibitor molecules demonstrate significant interaction with the metal surface, a result further validated by Mulliken Atomic Charge (MAC) analysis [62,63,75,76]. In particular, the oxygen and nitrogen atoms within the inhibitor structures play a crucial role in these interactions. This finding is consistent with previous studies, which have highlighted the strong affinity of oxygen- and nitrogen-containing functional groups for metal surfaces, often forming stable coordination bonds with surface atoms [31,42].

Therefore, it can be concluded that these heteroatoms - and especially the hydroxyl groups - contribute substantially to the inhibition mechanism, a conclusion also supported by molecular dynamics (MD) simulation outcomes. Monte Carlo simulation results reveal distinct adsorption energy profiles for each inhibitor molecule, reflecting differences in their affinity toward the metal surface.

As shown in Fig. 11, Rutin exhibits the most negative adsorption energies, predominantly clustered in the range of –324 to –270 kcal/mol, indicating strong and stable adsorption, which is suggestive of a high corrosion inhibition efficiency. Similarly, Myricetin displays a narrow distribution of energies centered around –270 to –216 kcal/mol, reflecting consistent and favorable interaction with the surface. Tenoxin shows a moderate adsorption profile, with most energies falling within the –270 to –216 kcal/mol range, suggesting a relatively stable, though less pronounced, surface interaction

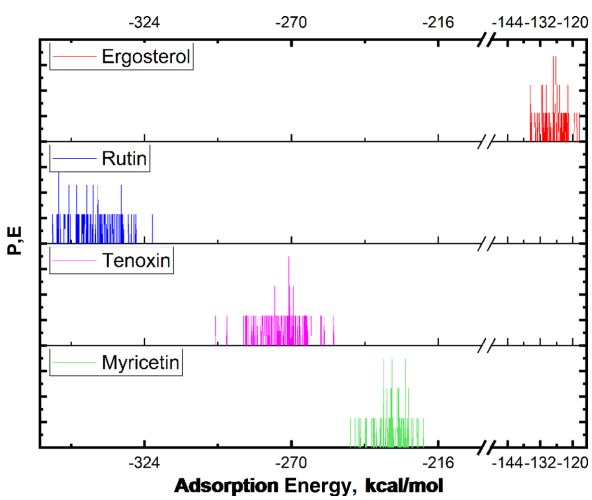

Fig. 11. Distribution of the adsorption energies for the studied inhibitors obtained via MC

compared to Rutin and Myricetin. In contrast, Ergosterol demonstrates significantly weaker adsorption, with energies mostly clustered around –144 to –120 kcal/mol, indicating physisorption-like behavior and a comparatively lower inhibition potential. The adsorption of inhibitor molecules onto the metal surface can lead to the formation of a protective layer that enhances the surface's resistance to corrosion. This effect is primarily attributed to the high adsorption energies exhibited by the inhibitors, as illustrated in Fig. 11. These energies reflect strong interactions between the inhibitor molecules and the metal surface, facilitating stable adsorption. Initiated by the metal's surface properties, this process results in the development of a compact and adherent molecular film that acts as a barrier against corrosive agents, thereby helping to preserve the metal in its original, uncorroded state [77-84].

In most publications, theoretical computations of inhibitors in the context of plant and other extracts are typically conducted by treating the components as isolated entities. However, in this study, we have advanced the complexity by considering more realistic scenarios, where the individual components of the extract interact simultaneously with the MS surface. This approach not only reflects more accurately the conditions encountered in practical applications but also allows us to explore the synergistic effects of the extract's components. As observed in both cases, the molecules are positioned in close proximity to the surface, which aligns with their relatively large adsorptive interaction energies, indicating strong and favorable interactions. These findings highlight the significance of collective interactions among extract components and their potential for more effective surface adsorption. Molecular dynamics (MD) simulations are widely regarded as a reliable and accurate approach for investigating adsorption phenomena on metal surfaces [46,51,73,85].

This perspective is supported by previous research demonstrating that MD simulation outcomes can be effectively validated through comparison with both experimental data and theoretical predictions [42,71,86]. The current findings reinforce the idea that the adsorption of inhibitor molecules onto metallic surfaces plays a crucial role in enhancing corrosion resistance, with MD simulations serving as a powerful tool for exploring these interactions at the atomic level. Within the context of MD,

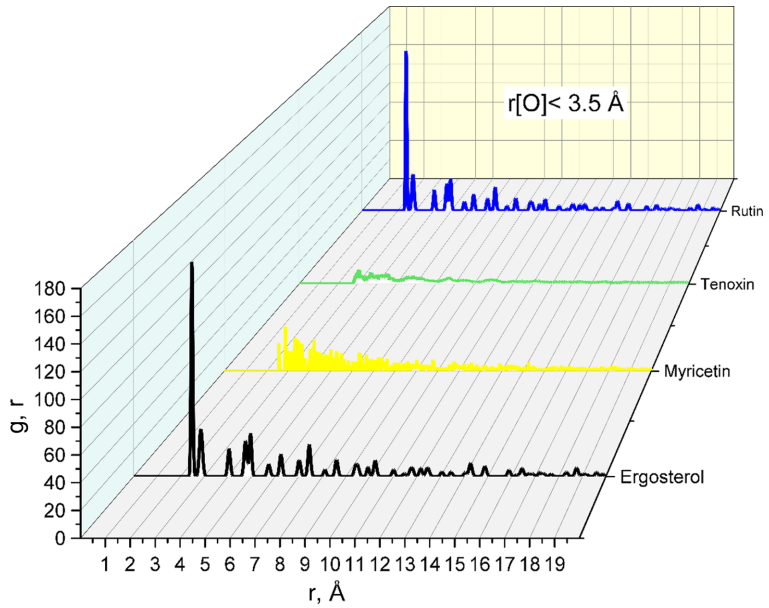

Fig. 12. RDF graph for the O atoms of the analyzed corrosion inhibitors of the TVE extract

the radial distribution function (RDF) is particularly valuable for examining molecular interactions with surfaces [9,87,88]. Commonly denoted as "g(r)" the RDF provides insight into the spatial distribution and structural organization of atoms or molecules, and its significance in adsorption studies is well-documented in the literature [33,39,42]. Our results, presented in Fig. 12, reveal that the oxygen atoms of these inhibitors are located within 3.5 Å of the metal surface, as indicated by the RDF analysis conducted in this study. This proximity underscores the key interaction patterns between the inhibitors and the metal surface, highlighting the strength and specificity of these interactions.

3.7 The Study of the Film Density and the Self-Diffusion Coefficients of corrosive species inside the inhibitor film

After the molecular dynamics (MD) simulations, the density values of the inhibitor-formed films were collected, and their average values are summarized in Table 3.

Table 3. Parameters for corrosion thin-film model construction

a = b = c [Å]	α = β = γ [°]	Density [g/cm^3]	Number of Molecules
43.62	90	0.990	2500 water 2 of each inhibitors 10 chloride 10 hydronium ions

The determination of the diffusion coefficient is calculated by equation (14) [70]:

$$D = \frac{1}{6}\lim_{t\to\infty}\sum_{i=1}^{N\alpha}\langle(r_i(t)-r_i(0))^2\rangle \quad (14)$$

where the $\langle(r_i(t)-r_i(0))^2\rangle$ is the mean squared displacement values obtained from MD trajectory.

Inhibitors influence the movement of corrosive ions - such as hydronium and chloride - at the interface of the inhibitor film. Interactions like van der Waals and Coulomb forces can shift the positions of the film-forming inhibitor molecules within the corrosive environment, altering the voids and structure of the film. These changes directly impact how easily corrosive ions can move through the film.

At the interface of the inhibitor-formed film, the mobility of corrosive ions - such as hydronium and hydronium ions - is significantly influenced by the mobility of the inhibitor molecules themselves. These film-forming inhibitors interact with the corrosive environment through van der Waals and Coulomb forces, which can cause their displacement within the film. As a result, the volume and shape of the film's internal cavities are altered, directly affecting the diffusion pathways

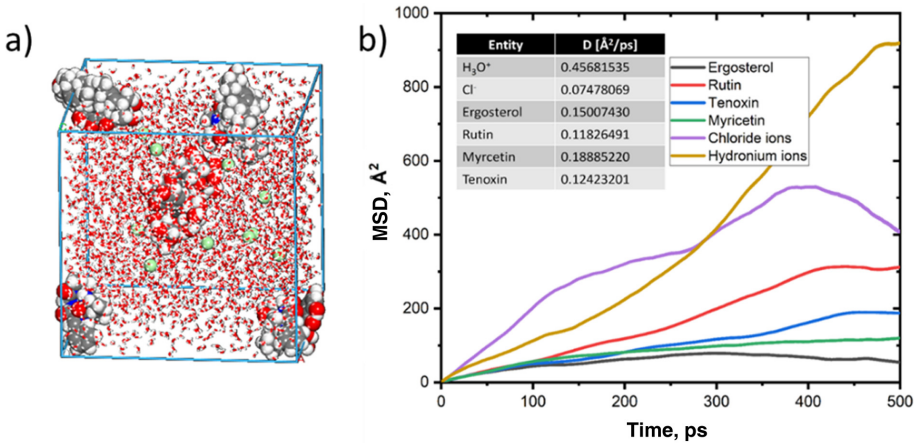

Fig. 13. a) The molecular dynamics (MD) simulation box setup, and b) the mean squared displacement (MSD) trajectories used for calculating the diffusion coefficients of the inhibitors and corrosive species

available to corrosive ions. A film with higher molecular mobility typically allows for greater ion diffusion, as reflected by a larger diffusion coefficient. The observed variation in diffusivity among the studied species can be attributed to differences in molecular size, charge, and interaction dynamics within the inhibitor film matrix. Hydronium ions exhibit the highest diffusivity (0.465 Å/ps), consistent with their small size and the well-known Grotthuss proton-hopping mechanism [89], which facilitates rapid mobility even in confined environments. In contrast, chloride ions display a lower diffusivity (0.0747 $Å^2$/ps), likely due to their larger ionic radius and stronger electrostatic interactions with the surrounding medium, which hinder their movement. The organic film-forming inhibitor molecules exhibit diffusivities in the range of 0.10-0.18 $Å^2$/ps (Fig. 13), reflecting their larger molecular structures and the stabilizing van der Waals and Coulombic interactions they engage in within the film. These interactions reduce their dynamic freedom, thereby limiting their overall mobility. Thus, their accumulation (due to adsorption) in the nearby vicinity of the metal surface acts as a barrier that prevents the corrosive species from interacting with the surface, thereby offering surface protection.

3.8 QSAR Modeling Results

Using R software [56] the correlation matrix and multiple regression analysis among all of the the computed QSAR inhibitor properties vs. Eads. Quantitative Structure–Activity Relationship (QSAR) modeling was employed to correlate molecular descriptors of the bioactive compounds in the *Trametes versicolor* extract with their adsorption energy ($E_{ads.}$), obtained from Monte Carlo simulations. The aim was to predict corrosion inhibition performance based on molecular structure. The following steps were undertaken: A. Descriptor Selection: 22 descriptors (W_1 to W_{22}) were initially considered, ranging from quantum chemical (HOMO, LUMO, dipole) to topological and spatial descriptors (Zagreb, Wiener indices), and B. Dimensionality Reduction: Due to multicollinearity and limited data (only 4 molecules: rutin, myricetin, tentoxin, ergosterol), only four independent variables were retained: W_1: Co nnolly surface area; W_2: Connolly surface volume; W_3: HOMO, and W_4: LUMO (the retained descriptors are physicochemically relevant: Connolly area/volume relate to surface accessibility and adsorption potential and the HOMO/LUMO reflect electron-donating/accepting abilities, crucial for metal surface interactions).

$$\hat{A} = \begin{bmatrix} 0 \\ -0.743178701 \\ 0 \\ 0.578167981 \\ 0.597721025 \end{bmatrix}$$

and so: $\hat{Y}_P = -0.743178701X_{1p} + 0.578167981X_{3p} + 0.597721025X_{4p}$; p = 1, 2, 3, 4.

The following table shows the variance for multiple linear regression.

Analysis of Variance Table for Linear Multiple Regression

Source of Variance	Degree of Freedom	Sum of Squares	Means Squares
Total	T-1	$SST = \sum (Y_j - \bar{y})^2$	$MST = \frac{SST}{T-1}$
Regression	n	$SST = \sum (Y_j - \bar{Y})^2$	$MSR = \frac{SSR}{p}$
Error	T-n-1	$SST = \sum (Y_j - Y_j)^2$	$MSE = \frac{SSE}{T-n-1}$

The coefficient of determination and the correlation coefficient are given by:

$$r^2 = 1 - \frac{SSE}{SST} \text{ and } r = \sqrt{1 - \frac{SSE}{SST}}.$$

In our case: $r^2 = 1 \Rightarrow r = 1$ The multiple regression QSAR analysis provides meaningful mechanistic insight into the molecular determinants of corrosion inhibition. While preliminary due to the small dataset, it establishes a valuable framework for screening and optimizing natural inhibitors using QSAR descriptors.

3.9 Adsorption Mechanism

The molecules identified in TVE, as supported by existing literature, strongly support the well-established mechanism of corrosion inhibition under acidic conditions. The text outlines that these inhibitor molecules can adhere to the metal surface through four primary modes of adsorption: (1) electrostatic attraction between charged inhibitor species and the charged metal surface; (2) coordination between lone electron pairs on the molecule and vacant orbitals on the metal; (3) interactions involving π-electrons from conjugated systems; and (4) a synergistic combination of these mechanisms.

For physical adsorption to effectively take place in an acidic medium, two essential conditions must be met: the metal surface must have available empty orbitals, and the surrounding solution should contain charged or polarizable species - such as molecules with delocalized electrons or heteroatoms bearing lone electron pairs. As depicted in Fig. 14, the studied inhibitors generally operate through a combined physisorption–chemisorption mechanism. Although scanning electron microscopy (SEM) analysis was not available during the present study, similar investigations using plant- and fungi-based corrosion

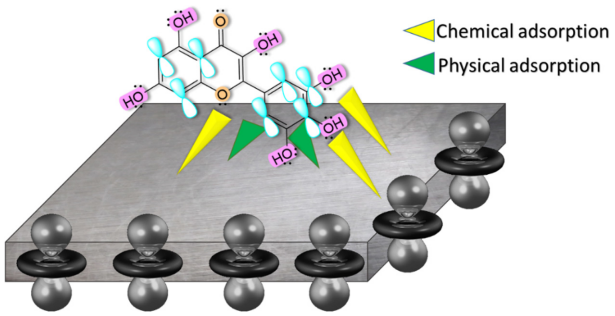

Fig. 14. Pictorial diagram of the adsorption mechanism (Myricetin molecule taken as an example)

inhibitors have consistently shown that such bioactive compounds form protective films that result in smoother and more uniform steel surfaces. These films typically reduce surface roughness and minimize pit formation caused by acidic corrosion. As supported by literature [90], the adsorption of flavonoids and polyphenols onto mild steel creates a compact barrier layer, which aligns with our proposed mechanism of inhibitor action for the compounds present in the *Trametes versicolor* extract.

4. Conclusion

This study comprehensively investigated the corrosion inhibition potential of *Trametes versicolor* (Turkey Tail Mushroom) extract on mild steel in a 1 M HCl solution using a synergistic experimental–theoretical approach. Gravimetric measurements demonstrated excellent inhibition efficiency, reaching 92.1% at 800 mg/L, with performance decreasing at elevated temperatures—consistent with a physisorption-dominated mechanism. Chemical and spectroscopic analyses (GC-MS/MS, FTIR, and UV-Vis) revealed a diverse array of bioactive compounds—particularly flavonoids such as myricetin and rutin—featuring functional groups (hydroxyl,

carbonyl, and amine) known for their affinity toward metal surfaces. Computational methods including density functional theory (DFT), Monte Carlo (MC), and molecular dynamics (MD) simulations confirmed strong interactions between the extract's active constituents and the Fe(110) surface, particularly through electron donation and hydrogen bonding. Among the compounds studied, myricetin exhibited superior electronic characteristics and adsorption behavior, aligning well with experimental observations. To further elucidate structure–activity relationships, a quantitative structure–activity relationship (QSAR) model was constructed using 22 molecular descriptors. The model identified frontier orbital energies and molecular surface parameters as critical predictors of adsorption energy, highlighting the potential of QSAR tools in guiding the rational design of green inhibitors. *Trametes versicolor* extract emerges as a sustainable, non-toxic, and effective corrosion inhibitor. The integration of experimental techniques with advanced theoretical modeling offers a robust framework for future screening, optimization, and application of bio-derived inhibitors in industrial corrosion control.

Acknowledgments

This study was supported by the University of Prishtina through the project entitled "The Power of Mushroom Extracts: Kosovo's New Green Corrosion Inhibitors" The authors also gratefully acknowledge the support of the Ministry of Education, Science, Technology, and Innovation (MESTI) of Kosovo (Grant No. 2-5069) for providing the computational resources necessary for this research.

References

1. C. Verma, E. E. Ebenso, M. A. Quraishi, Ionic liquids as green and sustainable corrosion inhibitors for metals and alloys: An overview, *Journal of Molecular Liquids*, **233**, 403 (2017). Doi: https://doi.org/10.1016/j.molliq.2017.02.111
2. S. Tanwer, S. K. Shukla, Recent advances in the applicability of drugs as corrosion inhibitor on metal surface: A review, *Current Research in Green and Sustainable Chemistry*, **5**, 100227 (2022). Doi: https://doi.org/10.1016/J.CRGSC.2021.100227
3. H. Wei, B. Heidarshenas, L. Zhou, G. Hussain, Q. Li, K. (Ken) Ostrikov, Green inhibitors for steel corrosion in acidic environment: state of art, *Materials Today Sustainability*, **10**, 100044 (2020). Doi: https://doi.org/10.1016/j.mtsust.2020.100044
4. B. Sanyal, Organic compounds as corrosion inhibitors in different environments — A review, *Progress in Organic Coatings*, **9**, 165 (1981). Doi: https://doi.org/10.1016/0033-0655(81)80009-X
5. A. Berisha, An Experimental and Theoretical Investigation of the Efficacy of Pantoprazole as a Corrosion Inhibitor for Mild Steel in an Acidic Medium, *Electrochem,* **3**, 28 (2022). Doi: https://doi.org/10.3390/electrochem3010002
6. R. Hsissou, S. Abbout, R. Seghiri, M. Rehioui, A. Berisha, H. Erramli, M. Assouag, A. Elharfi, Evaluation of corrosion inhibition performance of phosphorus polymer for carbon steel in [1 M] HCl: Computational studies (DFT, MC and MD simulations), *Journal of Materials Research and Technology*, **9**, 2691 (2020). Doi: https://doi.org/10.1016/j.jmrt.2020.01.002
7. A. Molhi, R. Hsissou, M. Damej, A. Berisha, V. Thaçi, A. Belafhaili, M. Benmessaoud, N. Labjar, S. El Hajjaji, Contribution to the corrosion inhibition of c38 steel in 1 m hydrochloric acid medium by a new epoxy resin pgeppp, *International Journal of Corrosion and Scale Inhibition*, **10**, 399 (2021). Doi: https://doi.org/10.17675/2305-6894-2021-10-1-23
8. A. Thakur, O. Dagdag, A. Berisha, E. Ebenso, A. Kumar, S. Sharma, R. Ganjoo, H. Assad, Experimental accompanied with computational (atomic/electronic)-level simulation investigations of Polygonum cuspidatum root extract as sustainable corrosion inhibitor for mild steel in aggressive corrosive media, *Environmental Science and Pollution Research*, **32**, 17059 (2024). Doi: https://jglobal.jst.go.jp/en/detail?JGLOBAL_ID=202502230755966115
9. B. Ould Abdelwedoud, M. Damej, K. Tassaoui, A. Berisha, H. Tachallait, K. Bougrin, V. Mehmeti, M. Benmessaoud, Inhibition effect of N-propargyl saccharin as corrosion inhibitor of C38 steel in 1 M HCl, experimental and theoretical study, *Journal of Molecular Liquids*, **354**, 118784 (2022). Doi: https://doi.org/10.1016/j.molliq.2022.118784
10. C. Verma, E.E. Ebenso, M.A. Quraishi, C.M. Hussain, Recent developments in sustainable corrosion inhibitors: design, performance and industrial scale applications, *Materials Advances*, **2**, 3806 (2021). Doi: https://doi.org/10.1039/D0MA00681E

11. A. A. Farag, Applications of nanomaterials in corrosion protection coatings and inhibitors, *Corrosion Reviews*, **38**, 67 (2020). Doi: https://doi.org/10.1515/corrrev-2019-0011
12. I. Eliboev, E. Berdimurodov, K. Yakhshinorov, J. Abdisattarov, O. Dagdag, A. Berisha, W. B. W. Nik, A. Kholikov, K. Akbarov, Supramolecular corrosion protection: Eco-friendly synthesis and efficacy of a β-cyclodextrin/o-phenylenediamine complex, *Journal of the Taiwan Institute of Chemical Engineers*, **147**, 104944 (2023). Doi: https://doi.org/10.1016/J.JTICE.2023.104944
13. S. El Arrouji, K. Karrouchi, A. Berisha, K. Ismaily Alaoui, I. Warad, Z. Rais, S. Radi, M. Taleb, M. Ansar, A. Zarrouk, New pyrazole derivatives as effective corrosion inhibitors on steel-electrolyte interface in 1 M HCl: Electrochemical, surface morphological (SEM) and computational analysis, *Colloids and Surfaces A: Physicochemical and Engineering Aspects*, **604**, 125325 (2020). Doi: https://doi.org/10.1016/j.colsurfa.2020.125325
14. D. Iravani, N. Esmaeili, A. Berisha, E. Akbarinezhad, M.H. Aliabadi, The quaternary ammonium salts as corrosion inhibitors for X65 carbon steel under sour environment in NACE 1D182 solution: Experimental and computational studies, *Colloids and Surfaces A: Physicochemical and Engineering Aspects*, **656**, 130544 (2023). Doi: https://doi.org/10.1016/j.colsurfa.2022.130544
15. P.K. Uppalapati, A. Berisha, K. Velmurugan, R. Nandhakumar, A. Khosla, T. Liang, Salen type additives as corrosion mitigator for Ni–W alloys: Detailed electronic/atomic-scale computational illustration, *International Journal of Quantum Chemistry*, **121**, e26600 (2021). Doi: https://doi.org/10.1002/qua.26600
16. S. Dadou, A. Elyoussfi, O. Dagdag, M. Koudad, J. Isaad, H. Kim, A. Berisha, I. Azghay, A. Salhi, M. Ahari, S. El Barkany, H. Amhamdi, N. Benchat, A. Dafali, The impact of halogen substitution on the corrosion inhibition of imidazothiazole derivatives for mild steel in corrosive media (Part A), *Colloids and Surfaces A: Physicochemical and Engineering Aspects*, **687**, 133451 (2024). Doi: https://doi.org/10.1016/j.colsurfa.2024.133451
17. R. Hsissou, F. Benhiba, S. Echihi, S. Benkhaya, M. Hilali, A. Berisha, S. Briche, A. Zarrouk, K. Nouneh, A. Elharfi, New epoxy composite polymers as a potential anticorrosive coatings for carbon steel in 3.5% NaCl solution: Experimental and computational approaches, *Chemical Data Collections*, **31**, 100619 (2021). Doi: https://doi.org/10.1016/j.cdc.2020.100619
18. M. Rbaa, P. Dohare, A. Berisha, O. Dagdag, L. Lakhrissi, M. Galai, B. Lakhrissi, M.E. Touhami, I. Warad, A. Zarrouk, New Epoxy sugar based glucose derivatives as eco friendly corrosion inhibitors for the carbon steel in 1.0 M HCl: Experimental and theoretical investigations, *Journal of Alloys and Compdounds*, **833**, 154949 (2020). Doi. https://doi.org/10.1016/j.jallcom.2020.154949
19. S. Abbout, R. Hsissou, D. Chebabe, H. Erramli, Z. Safi, N. Wazzan, A. Berisha, A. Reka, N. Hajjaji, Investigation of Two Corrosion Inhibitors in Acidic Medium Using Weight Loss, Electrochemical Study, Surface Analysis, and Computational Calculation, *Journal of Bio- and Tribo-Corrosion*, **8**, 86 (2022). Doi: https://doi.org/10.1007/s40735-022-00684-y
20. A. Molhi, R. Hsissou, M. Damej, A. Berisha, V. Thaçi, A. Belafhaili, M. Benmessaoud, N. Labjar, S. El Hajjaji, Contribution to the corrosion inhibition of C38 steel in 1 M hydrochloric acid medium by a new epoxy resin PGEPPP, *International Journal of Corrosion and Scale Inhibition*, **10**, 399 (2021). Doi: https://doi.org/10.17675/2305-6894-2021-10-1-23
21. H. Jafari, E. Ameri, M. Rezaeivala, A. Berisha, Experimental and theoretical studies on protecting steel against 0.5 M H2SO4 corrosion by new schiff base, *Journal of the Indian Chemical Society*, **99**, 100665 (2022). Doi: https://doi.org/10.1016/j.jics.2022.100665
22. N. B. Iroha, V. C. Anadebe, N. J. Maduelosi, L. A. Nnanna, L. C. Isaiah, O. Dagdag, A. Berisha, E. E. Ebenso, Linagliptin drug molecule as corrosion inhibitor for mild steel in 1 M HCl solution: Electrochemical, SEM/XPS, DFT and MC/MD simulation approach, *Colloids Surfaces A: Physicochemical and Engineering Aspects*, **660**, 130885 (2023). Doi: https://doi.org/10.1016/j.colsurfa.2022.130885
23. G. Cui, Z. Bi, S. Wang, J. Liu, X. Xing, Z. Li, B. Wang, A comprehensive review on smart anti-corrosive coatings, *Progress in Organic Coatings*, **148**, 105821 (2020). Doi: https://doi.org/10.1016/J.PORGCOAT.2020.105821
24. M. Abouchane, R. Hsissou, A. Chraka, A. Molhi, M. Damej, K. Tassaoui, A. Berisha, M. Seydou, B.O. Elemine, M. Benmessaoud, Synthesis and Characterization of New Macromolecular Epoxy Resin as an Effective Corrosion Inhibitor for C38 Steel in 1 M HCl Medium: Electrochemical Insights, Surface Morphological and Computational Approaches, *Journal of Bio-and Tribo-Corrosion*, **10**, 21 (2024). Doi: https://doi.org/10.1007/s40735-024-00824-6

25. W. Daoudi, O. Dagdag, C. Verma, E. Berdimurodov, A. Oussaid, A. Berisha, A. Oussaid, M. Abboud, A. El Aatiaoui, Rosmarinus officinalis l. Oil as an Eco-Friendly corrosion inhibitor for mild steel in acidic Solution: Experimental and computational studies, *Inorganic Chemistry Communications*, **161**, 112030 (2024). Doi: https://doi.org/10.1016/j.inoche.2024.112030
26. A. Thakur, O. Dagdag, A. Berisha, E. E. Ebenso, A. Kumar, S. Sharma, R. Ganjoo, H. Assad, Mechanistic insights into the corrosion inhibition of mild steel by eco-benign Asphodelus Tenuifolius aerial extract in acidic environment: Electrochemical and computational analysis, *Surface and Coatings Technology*, **480**, 130568 (2024). Doi: https://doi.org/10.1016/j.surfcoat.2024.130568
27. C. Verma, E. E. Ebenso, I. Bahadur, M. A. Quraishi, An overview on plant extracts as environmental sustainable and green corrosion inhibitors for metals and alloys in aggressive corrosive media, *Journal of Molecular Liquids*, **266**, 577 (2018). Doi: https://doi.org/10.1016/j.molliq.2018.06.110
28. R. Suarez-Hernandez, G. F. Dominguez-Patiño, J. G. Gonzalez-Rodriguez, I. Tello, V. M. Salinas-Bravo, J. G. Chacon-Nava, Use of Reishi Mushroom Extract as Green Corrosion Inhibitor for Carbon Steel in Acid Media, *Journal of Natural Products and Resources*, **2**, 58 (2016). https://www.researchgate.net/publication/332333344_Use_of_Reishi_Mushroom_Extract_as_Green_Corrosion_Inhibitor_for_Carbon_Steel_in_Acid_Media
29. F. Ivušić, Higher fungi extracts as inhibitors of carbon steel corrosion in chloride rich environment, *International Journal of Corrosion and Scale Inhibition*, **11**, 161 (2022). Doi: https://doi.org/10.17675/2305-6894-2022-11-1-9
30. G. P. Monteiro, I. M. de C. Tavares, M. C. F. de Carvalho, M. S. Carvalho, A. B. Pimentel, P. H. Santos, E. V. de B. Vilas Boas, J. R. de Oliveira, V. R. Capelossi, M. Bilal, M. Franco, Evaluation of fungal biomass developed from cocoa by-product as a substrate with corrosion inhibitor for carbon steel, *Chemical Engineering Communications*, **210**, 1207 (2023). Doi: https://doi.org/10.1080/00986445.2022.2073228
31. R. Ganjoo, S. Sharma, P. K. Sharma, O. Dagdag, A. Berisha, E. E. Ebenso, A. Kumar, C. Verma, Coco Monoethanolamide Surfactant as a Sustainable Corrosion Inhibitor for Mild Steel: Theoretical and Experimental Investigations, *Molecules*, **28**, 1581 (2023). Doi: https://doi.org/10.3390/MOLECULES28041581
32. A. Benallal, M. Rbaa, Z. Rouifi, M. Galai, N. Errahmany, E. Berdimurodov, V. Mehmeti, A. Berisha, S.I. Ahmed, I. Warad, A. Zarrouk, Quinoxaline Derivatives as Newly Acid Corrosion Inhibitors for Mild Steel: Synthesis, Electrochemical, and Theoretical Investigations, *Journal of Bio- and Tribo-Corrosion*, **9**, 30 (2023). Doi: https://doi.org/10.1007/S40735-023-00750-Z
33. R. Ihamdane, M. Tiskar, B. Outemsaa, L. Zelmat, O. Dagdag, A. Berisha, E. Berdimurodov, E.E. Ebenso, A. Chaouch, Essential Oil of Origanum vulgare as a Green Corrosion Inhibitor for Carbon Steel in Acidic Medium, *Arabian Journal for Science and Engineering*, **48**, 7685 (2023). Doi: https://doi.org/10.1007/S13369-023-07693-0
34. F. Mohsenifar, H. Jafari, K. Sayin, Investigation of Thermodynamic Parameters for Steel Corrosion in Acidic Solution in the Presence of N,N′-Bis(phloroacetophenone)-1,2 propanediamine, *Journal of Bio- and Tribo-Corrosion*, **2**, 1 (2016). Doi: https://doi.org/10.1007/s40735-015-0031-y
35. A. Molhi, R. Hsissou, M. Damej, A. Berisha, M. Bamaarouf, M. Seydou, M. Benmessaoud, S. El Hajjaji, Performance of two epoxy compounds against corrosion of C38 steel in 1 M HCl: Electrochemical, thermodynamic and theoretical assessment, *Internationl Journal of Corrosion and Scale Inhibition*, **10**, 812 (2021). Doi: https://doi.org/10.17675/2305-6894-2021-10-2-21
36. H. Jafari, E. Ameri, F. Soltanolkottabi, A. Berisha, M. Seydou, Experimental and theoretical investigations of new Schiff base compound adsorption on aluminium in 1 M HCl, *Journal of Electrochemical Science and Engineering*, **12**, 975 (2022). Doi: https://doi.org/10.5599/jese.1405
37. A. Farhadian, Y. Zhao, P. Naeiji, A. Rahimi, A. Berisha, L. Zhang, Z.T. Rizi, D. Iravani, J. Zhao, Simultaneous inhibition of natural gas hydrate formation and CO2/H2S corrosion for flow assurance inside the oil and gas pipelines, *Energy*, **269**, 126797 (2023). Doi: https://doi.org/10.1016/J.ENERGY.2023.126797
38. K. Zaidi, A. Aouniti, C. Merimi, W. Daoudi, O. Dagdag, A. Berisha, A. Oussaid, R. Touzani, M. Messali, B. Hammouti, Comparative study of inhibitory efficacy of methionine and its derivatives in acidic medium by mild steel, *Moroccan Journal of Chemistry*, **11**, 411 (2023). Doi: https://doi.org/10.48317/IMIST.PRSM/MORJCHEM-V11I2.38246
39. D. Iravani, N. Esmaeili, A. Berisha, E. Akbarinezhad, M. H. Aliabadi, The quaternary ammonium salts as corro-

sion inhibitors for X65 carbon steel under sour environment in NACE 1D182 solution: Experimental and computational studies, *Colloids and Surfaces A: Physicochemical and Engineering Aspects*, **656**, 130544 (2023). Doi: https://doi.org/10.1016/J.COLSURFA.2022.130544

40. C. Tang, A. Farhadian, A. Berisha, M. A. Deyab, J. Chen, D. Iravani, A. Rahimi, Z. Zhang, D. Liang, Novel Biosurfactants for Effective Inhibition of Gas Hydrate Agglomeration and Corrosion in Offshore Oil and Gas Pipelines, *ACS Sustainable Chemistry & Engineering*, **11**, 353 (2023). Doi: https://doi.org/10.1021/acssuschemeng.2c05716
41. R. Haldhar, C. Jayprakash Raorane, V.K.K. Mishra, T. Periyasamy, A. Berisha, S.-C.S.C. Kim, Development of different chain lengths ionic liquids as green corrosion inhibitors for oil and gas industries: Experimental and theoretical investigations, *Journal of Molecular Liquids*, **372**, 121168 (2023). Doi: https://doi.org/10.1016/J.MOLLIQ.2022.121168
42. M. Alahiane, R. Oukhrib, Y. Ait Albrimi, H. Abou Oualid, R. Idouhli, A. Nahlé, A. Berisha, N. Z. Azzallou, M. Hamdani, Corrosion inhibition of SS 316L by organic compounds: Experimental, molecular dynamics, and conceptualization of molecules–surface bonding in H2SO4 solution, *Applied Surface Science*, **612**, 155755 (2023). Doi: https://doi.org/10.1016/j.apsusc.2022.155755
43. R. L. C. Akkermans, N. A. Spenley, S. H. Robertson, COMPASS III: automated fitting workflows and extension to ionic liquids, *Molecular Simulation*, **47**, 540 (2020). Doi: https://doi.org/10.1080/08927022.2020.1808215
44. H. Sun, Z. Jin, C. Yang, R.L.C. Akkermans, S.H. Robertson, N.A. Spenley, S. Miller, S.M. Todd, COMPASS II: extended coverage for polymer and drug-like molecule databases, *Journal of Molecular Modeling*, **22**, 1 (2016). Doi: https://doi.org/10.1007/s00894-016-2909-0
45. H. Lgaz, R. Salghi, A. Chaouiki, Shubhalaxmi, S. Jodeh, K. Subrahmanya Bhat, Pyrazoline derivatives as possible corrosion inhibitors for mild steel in acidic media: A combined experimental and theoretical approach, *Cogent Engineering*, **5**, Article no. 1441585 (2018). Doi: https://doi.org/10.1080/23311916.2018.1441585
46. A. Ouass, M. Galai, M. Ouakki, E. Ech-Chihbi, L. Kadiri, R. Hsissou, Y. Essaadaoui, A. Berisha, M. Cherkaoui, A. Lebkiri, E.H. Rifi, Poly(sodium acrylate) and Poly(acrylic acid sodium) as an eco-friendly corrosion inhibitor of mild steel in normal hydrochloric acid: experimental, spectroscopic and theoretical approach, *Journal of Applied Electrochemistry*, **51**, 1009 (2021). Doi: https://link.springer.com/article/10.1007/s10800-021-01556-y
47. O. Amrhar, A. Berisha, L. El Gana, H. Nassali, M. S. Elyoubi, Removal of methylene blue dye by adsorption onto Natural Muscovite Clay: experimental, theoretical and computational investigation, *International Journal of Environmental Analytical Chemistry*, **103**, 2419 (2023). Doi: https://doi.org/10.1080/03067319.2021.1897119
48. A. Berisha, Ab inito exploration of nanocars as potential corrosion inhibitors, *Computational and Theoretical Chemistry*, **1201**, 113258 (2021). Doi: https://linkinghub.elsevier.com/retrieve/pii/S2210271X21001171
49. O. Dagdag, A. El Harfi, L. El Gana, Z.S. Safi, L. Guo, A. Berisha, C. Verma, E. E. Ebenso, N. Wazzan, M. El Gouri, A. El Harfi, L. El Gana, Z. S. Safi, L. Guo, A. Berisha, C. Verma, E. E. Ebenso, N. Wazzan, M. El Gouri, Designing of phosphorous based highly functional dendrimeric macromolecular resin as an effective coating material for carbon steel in NaCl: Computational and experimental studies, *Journal of Applied Polymer Science*, **138**, 49673 (2021). Doi: https://onlinelibrary.wiley.com/doi/full/10.1002/app.49673
50. P. K. Uppalapati, A. Berisha, K. Velmurugan, R. Nandhakumar, A. Khosla, T. Liang, Salen type additives as corrosion mitigator for Ni–W alloys: Detailed electronic/atomic-scale computational illustration, *International Journal of Quantum Chemistry*, **121**, e26600 (2021). Doi: https://doi.org/10.1002/QUA.26600
51. M. El Faydy, H. About, I. Warad, Y. Kerroum, A. Berisha, F. Podvorica, F. Bentiss, G. Kaichouh, B. Lakhrissi, A. Zarrouk, Insight into the corrosion inhibition of new bis-quinolin-8-ols derivatives as highly efficient inhibitors for C35E steel in 0.5 M H_2SO_4, *Journal of Molecular Liquids*, **342**, 117333 (2021). Doi: https://doi.org/10.1016/J.MOLLIQ.2021.117333
52. J. Zhang, J. Liu, W. Yu, Y. Yan, L. You, L. Liu, Molecular modeling of the inhibition mechanism of 1-(2-aminoethyl)-2-alkyl-imidazoline, *Corrosion Science*, **52**, 2059 (2010). Doi: https://doi.org/10.1016/j.corsci.2010.02.018
53. A. Berisha, Experimental, Monte Carlo and Molecular Dynamic Study on Corrosion Inhibition of Mild Steel by Pyridine Derivatives in Aqueous Perchloric Acid, *Electrochem*, **1**, 188 (2020). Doi: https://doi.org/10.3390/electrochem1020013
54. K. Lopez, S. Pinheiro, W.J. Zamora, Multiple linear regression models for predicting the n-octanol/water partition coefficients in the SAMPL7 blind challenge, *Jour-*

nal of Computer-Aided Molecular Design, **35**, 923 (2021). Doi: https://doi.org/10.1007/S10822-021-00409-2

55. M. Krzywinski, N. Altman, Multiple linear regression, *Nature Methods*, **12**, 1103 (2015). Doi: https://doi.org/10.1038/nmeth.3665
56. A. Elsamman, K. F. Khaled, S. A. Halim, N. S. Abdelshafi, A critical view of the QSAR model for the prediction of a new bispyrazole derivative BPYR-P as a corrosion inhibitor for 304 SS in a 1.0 M HCl solution, *Journal of Molecular Structure*, **1297**, 136728 (2024). Doi: https://doi.org/10.1016/J.MOLSTRUC.2023.136728
57. S. Chen, D. Zhang, Study of corrosion behavior of copper in 3.5 wt.% NaCl solution containing extracellular polymeric substances of an aerotolerant sulphate-reducing bacteria, *Corrosion Science*, **136**, 275 (2018). Doi: https://doi.org/10.1016/J.CORSCI.2018.03.017
58. A. Zakeri, E. Bahmani, A.S.R. Aghdam, Plant extracts as sustainable and green corrosion inhibitors for protection of ferrous metals in corrosive media: A mini review, *Corrosion Communications*, **5**, 25 (2022). Doi: https://doi.org/10.1016/J.CORCOM.2022.03.002
59. A. Dehghani, P. Ghahremani, A. H. Mostafatabar, B. Ramezanzadeh, Plant extracts: Probable alternatives for traditional inhibitors for controlling alloys corrosion against acidic media—A review, *Biomass Conversion and Biorefinery*, **14**, 7467 (2022). Doi: https://doi.org/10.1007/S13399-022-02893-4
60. W. Daoudi, A. El Aatiaoui, O. Dagdag, K. Zaidi, R. Haldhar, S.-C. Kim, A. Oussaid, A. Aouinti, A. Berisha, F. Benhiba, E. E. Ebenso, A. Oussaid, Anti-Corrosion Coating Formation by a Biopolymeric Extract of Artemisia herba-alba Plant: Experimental and Theoretical Investigations, *Coatings*, **13**, 611 (2023). Doi. https://doi.org/10.3390/COATINGS13030611
61. W. Daoudi, A. El Aatiaoui, N. Falil, M. Azzouzi, A. Berisha, L. O. Olasunkanmi, O. Dagdag, E. E. Ebenso, M. Koudad, A. Aouinti, M. Loutou, A. Oussaid, Essential oil of Dysphania ambrosioides as a green corrosion inhibitor for mild steel in HCl solution, *Journal of Molecular Liquids*, **363**, 119839 (2022). Doi: https://doi.org/10.1016/j.molliq.2022.119839
62. R. Haldhar, S.-C.C. Kim, A. Berisha, V. Mehmeti, L. Guo, Corrosion inhibition abilities of phytochemicals: a combined computational studies, *Journal of Adhesion Science and Technology*, **37**, 842 Doi: https://doi.org/10.1080/01694243.2022.2047379
63. Z. Akounach, A. Al Maofari, M. Damej, S. El Hajjaji, A. Berisha, V. Mehmeti, N. Labjar, M. Bamaarouf, M. Benmessaoud, Contribution to the corrosion inhibition of aluminum in 1 M HCl by Pimpinella Anisum extract. Experimental and theoretical studies (DFT, MC, and MD), *International Journal of Corrosion and Scale Inhibition*, **11**, 402 (2022). Doi: https://doi.org/10.17675/2305-6894-2022-11-1-24
64. S. Lamghafri, W. Daoudi, A.E. Aatiaoui, O. Dagdag, H. Kim, A. Berisha, W.B.W. Nik, A.J. Obaidullah, K.K. Yadav, A. Zarrouk, A. Lamhamdi, Efficiency of alcohol and ester-imidazole in preventing mild steel corrosion: An integrated approach combining experimental and computational studies, *Journal of Molecular Structure*, **1306**, 137924 (2024). Doi: https://doi.org/10.1016/j.molstruc.2024.137924
65. S. Lamghafri, W. Daoudi, A. El Aatiaoui, O. Dagdag, H. Kim, F. Benhiba, A. Berisha, A. Barrahi, W.B.W. Nik, A. Zarrouk, A. Lamhamdi, Performance of Artemisia absinthium as an Ecological Corrosion Inhibitor in the Industrial Pickling Process, *Journal of Bio- and Tribo-Corrosion*, **10**, Article no. 17 (2024). Doi: https://doi.org/10.1007/s40735-023-00816-y
66. K. Haruna, T.A. Saleh, N,N′-Bis-(2-aminoethyl)piperazine functionalized graphene oxide (NAEP-GO) as an effective green corrosion inhibitor for simulated acidizing environment, *Journal of Environmental Chemical Engineering*, **9**, 104967 (2021). Doi: https://doi.org/10.1016/J.JECE.2020.104967
67. A. Klamt, The COSMO and COSMO-RS solvation models, *Wiley Interdisciplinary Reviews Computational Molecular Science*, **8**, e1338 (2018). Doi: https://doi.org/10.1002/wcms.1338
68. O. Dagdag, L. El Gana, R. Haldhar, A. Berisha, S.C. Kim, E. Berdimurodov, O. Hamed, S. Jodeh, E.D. Akpan, E.E. Ebenso, Study on Thermal Conductivity and Mechanical Properties of Cyclotriphosphazene Resin-Forced Epoxy Resin Composites, *Crystals*, **13**, 478 (2023). Doi: https://doi.org/10.3390/CRYST13030478/S1
69. W. Daoudi, O. Dagdag, C. Verma, E. Berdimurodov, A. Oussaid, A. Berisha, A. Oussaid, M. Abboud, A. El Aatiaoui, Rosmarinus officinalis l. Oil as an Eco-Friendly corrosion inhibitor for mild steel in acidic Solution: Experimental and computational studies, *Inorganic Chemistry Communications*, **161**, 112030 (2024). Doi: https://doi.org/10.1016/J.INOCHE.2024.112030
70. A. Berisha, Experimental, Monte Carlo and Molecular Dynamic Study on Corrosion Inhibition of Mild Steel by

Pyridine Derivatives in Aqueous Perchloric Acid, *Electrochem*, **1**, 188 (2020). Doi: https://doi.org/10.3390/electrochem1020013

71. R. Ganjoo, S. Sharma, A. Thakur, H. Assad, P. Kumar Sharma, O. Dagdag, A. Berisha, M. Seydou, E.E. Ebenso, A. Kumar, Experimental and theoretical study of Sodium Cocoyl Glycinate as corrosion inhibitor for mild steel in hydrochloric acid medium, *Journal of Molecular Liquids*, **364**, 119988 (2022). Doi: https://doi.org/10.1016/j.molliq.2022.119988
72. M. Damej, R. Hsissou, A. Berisha, K. Azgaou, M. Sadiku, M. Benmessaoud, N. Labjar, S. El hajjaji, New epoxy resin as a corrosion inhibitor for the protection of carbon steel C38 in 1M HCl. experimental and theoretical studies (DFT, MC, and MD), *Journal of Molecular Structure*, **1254**, 132425 (2022). Doi: https://doi.org/10.1016/j.molstruc.2022.132425
73. M. Alahiane, R. Oukhrib, A. Berisha, Y.A.Y.A. Albrimi, R.A.R.A. Akbour, H.A.H.A. Oualid, H. Bourzi, A. Assabbane, A. Nahlé, M. Hamdani, Electrochemical, thermodynamic and molecular dynamics studies of some benzoic acid derivatives on the corrosion inhibition of 316 stainless steel in HCl solutions, *Journal of Molecular Liquids*, **328**, 115413 (2021). Doi: https://doi.org/10.1016/j.molliq.2021.115413
74. R. Haldhar, D. Prasad, I. Bahadur, O. Dagdag, A. Berisha, Evaluation of Gloriosa superba seeds extract as corrosion inhibition for low carbon steel in sulfuric acidic medium: A combined experimental and computational studies, *Journal of Molecular Liquids*, **323**, 114958 (2021). Doi: https://doi.org/10.1016/J.MOLLIQ.2020.114958
75. H. Jafari, E. Ameri, M. Rezaeivala, A. Berisha, 4,4'-(((2,2-Dimethylpropane-1,3-Diyl)Bis(Azanediyl)Bis(Methylene) Bis(2-Methoxyphenol) as New Reduced Form of Schiff Base for Protecting API 5L Grade B in 1 M HCl, *Arabian Journal for Science and Engineering*, **48**, 7359 (2023). Doi: https://doi.org/10.1007/s13369-022-07281-8
76. K. Tassaoui, M. Damej, A. Molhi, A. Berisha, M. Errili, S. Ksama, V. Mehmeti, S. El Hajjaji, M. Benmessaoud, Contribution to the corrosion inhibition of Cu–30Ni copper–nickel alloy by 3-amino-1,2,4-triazole-5-thiol (ATT) in 3% NaCl solution. Experimental and theoretical study (DFT, MC and MD), *International Journal of Corrosion and Scale Inhibition*, **11**, 221 (2022). Doi: https://doi.org/10.17675/2305-6894-2022-11-1-12
77. A. Berisha, F. I. F. I. F. I. Podvorica, V. Mehmeti, F. Syla, D. Vataj, Theoretical and experimental studies of the corrosion behavior of some thiazole derivatives toward mild steel in sulfuric acid media, *Macedonian Journal of Chemistry and Chemical Engineering*, **34**, 287 (2015). Doi: https://doi.org/10.20450/mjcce.2015.576
78. L. Guo, C. Qi, X. Zheng, R. Zhang, X. Shen, S. Kaya, Toward understanding the adsorption mechanism of large size organic corrosion inhibitors on an Fe(110) surface using the DFTB method, *RSC Advances*, **7**, 29042 (2017). Doi: https://doi.org/10.1039/c7ra04120a
79. O. Dagdag, A. Berisha, Z. Safi, O. Hamed, S. Jodeh, C. Verma, E. E. E. Ebenso, A. El Harfi, DGEBA-polyaminoamide as effective anti-corrosive material for 15CDV6 steel in NaCl medium: Computational and experimental studies, *Journal of Applied Polymer Science*, **137**, 48402 (2020). Doi: https://doi.org/10.1002/app.48402
80. R. Hsissou, F. Benhiba, S. Abbout, O. Dagdag, S. Benkhaya, A. Berisha, H. Erramli, A. Elharfi, Trifunctional epoxy polymer as corrosion inhibition material for carbon steel in 1.0 M HCl: MD simulations, DFT and complexation computations, *Inorganic Chemistry Communications*, **115**, 107858 (2020). Doi: https://doi.org/10.1016/j.inoche.2020.107858
81. R. Hsissou, S. Abbout, A. Berisha, M. Berradi, M. Assouag, N. Hajjaji, A. Elharfi, Experimental, DFT and molecular dynamics simulation on the inhibition performance of the DGDCBA epoxy polymer against the corrosion of the E24 carbon steel in 1.0 M HCl solution, *Journal of Molecular Structure*, **1182**, 340 (2019). Doi: https://doi.org/10.1016/j.molstruc.2018.12.030
82. O. Dagdag, R. Hsissou, A. Berisha, H. Erramli, O. Hamed, S. Jodeh, A. El Harfi, Polymeric-Based Epoxy Cured with a Polyaminoamide as an Anticorrosive Coating for Aluminum 2024-T3 Surface: Experimental Studies Supported by Computational Modeling, *Journal of Bio- and Tribo-Corrosion*, **5**, Article no.58 (2019). Doi: https://doi.org/10.1007/s40735-019-0251-7
83. L.J. Yu, J. Zhang, G.M. Qiao, Y.G. Yan, Y. Ti, Y. Zhang, Effect of alkyl chain length on inhibition performance of imidazoline derivatives investigated by molecular dynamics simulation, *Materials and Corrosion*, **64**, 225 (2013). Doi: https://doi.org/10.1002/maco.201106141
84. V. V. Mehmeti, A.R. Berisha, Corrosion study of mild steel in aqueous sulfuric acid solution using 4-methyl-4h-1,2,4-triazole-3-thiol and 2-mercaptonicotinic acid-an experimental and theoretical study, *Frontiers in Chemistry*, **5**, 61 (2017). Doi: https://doi.org/10.3389/fchem.2017.00061
85. O. Dagdag, A. El Harfi, L. El Gana, Z. S. Safi, L. Guo,

A. Berisha, C. Verma, E.E. Ebenso, N. Wazzan, M. El Gouri, Designing of phosphorous based highly functional dendrimeric macromolecular resin as an effective coating material for carbon steel in NaCl: Computational and experimental studies, *Journal of Applied Polymer Sciemce*, **138**, 49673 (2021). Doi: https://doi.org/10.1002/app.49673

86. I. Lebkiri, B. Abbou, R. Hsissou, Z. Safi, M. Sadiku, A. Berisha, A. El Amri, Y. Essaadaoui, L. Kadiri, A. Lebkiri, E.H. Rifi, Investigation of the anionic polyacrylamide as a potential adsorbent of crystal violet dye from aqueous solution: Equilibrium, kinetic, thermodynamic, DFT, MC and MD approaches, *Journal of Molecular Liquids*, **372**, 121220 (2023). Doi: https://doi.org/10.1016/j.molliq.2023.121220
87. A. Rahimi, A. Farhadian, A. Berisha, A. Shaabani, M.A. Varfolomeev, V. Mehmeti, X. Zhong, S. Yousefzadeh, R. Djimasbe, Novel sucrose derivative as a thermally stable inhibitor for mild steel corrosion in 15% HCl medium: An experimental and computational study, *Chemical Engineering Journal*, **446**, 136938 (2022). Doi: https://doi.org/10.1016/j.cej.2022.136938
88. N. Bhardwaj, P. Sharma, A. Berisha, V. Mehmeti, O. Dagdag, V. Kumar, Monte Carlo simulation, molecular dynamic simulation, quantum chemical calculation and anti-corrosive behaviour of Citrus limetta pulp waste extract for stainless steel (SS-410) in acidic medium, *Materials Chemistry and Physics*, **284**, 126052 (2022). Doi: https://doi.org/10.1016/j.matchemphys.2022.126052
89. D. Marx, Proton Transfer 200 Years after von Grotthuss: Insights from Ab Initio Simulations, *ChemPhysChem*, **7**, 1848 (2006). Doi: https://doi.org/10.1002/CPHC.200600128
90. M. Gabsi, H. Ferkous, A. Delimi, A. Boublia, C. Boulechfar, A. Kahlouche, A.S. Darwish, T. Lemaoui, Y. Benguerba, The curious case of polyphenols as green corrosion inhibitors: a review on their extraction, design, and applications, *Environmental Science and Pollution Research*, **30**, 59081 (2023). Doi: https://doi.org/10.1007/S11356-023-26753-4